Nuclear Physics at the upgraded HIγS facility—An Introduction

Henry R. Weller

Duke University and Triangle Universities Nuclear Laboratory

HIγS PROGRAM

HUGS_1, June 2009

HIγS

- High Intensity γ-ray Source (HIγS)

–Located at the Duke Free Electron Laser Laboratory
--part of the Triangle Universities Nuclear Laboratory (TUNL)

–Intra-cavity Compton Back Scattering of FEL photons by electrons circulating in the Duke Storage Ring

HIγS

- ***Nearly Mono-energetic γ-rays***
  - —Tunable Energies
  - —Energy resolution selected by collimator size

- ***Linearly and Circularly Polarized γ-rays***

- ***High Beam Intensities***

- ***Pulsed Beam***
  - —TOF Techniques to reduce non-beam related backgrounds

One Bunch Mode

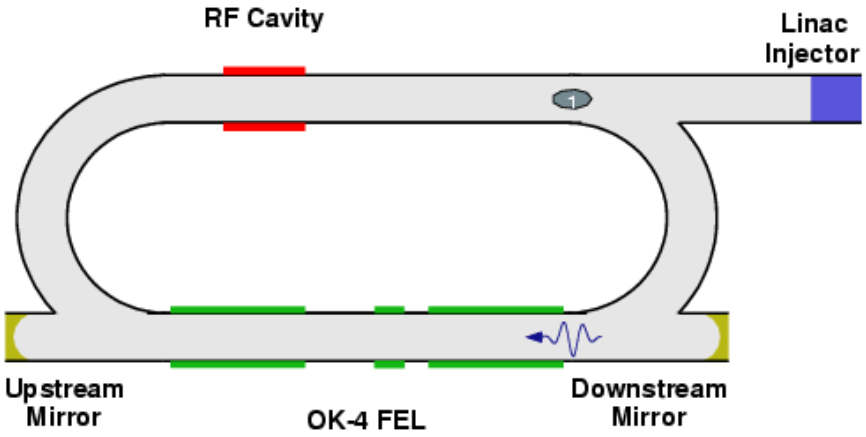

Created by Brent Perdue, 2005

Two Bunch Mode

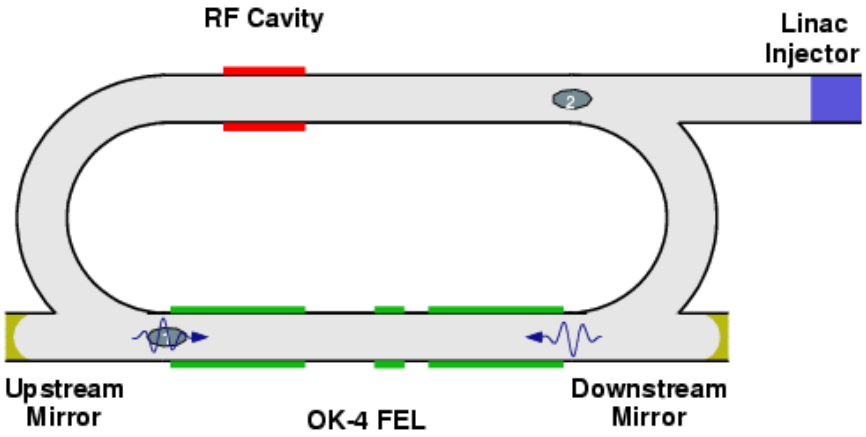

Created by Brent Perdue, 2005

γ-ray Production at HIγS

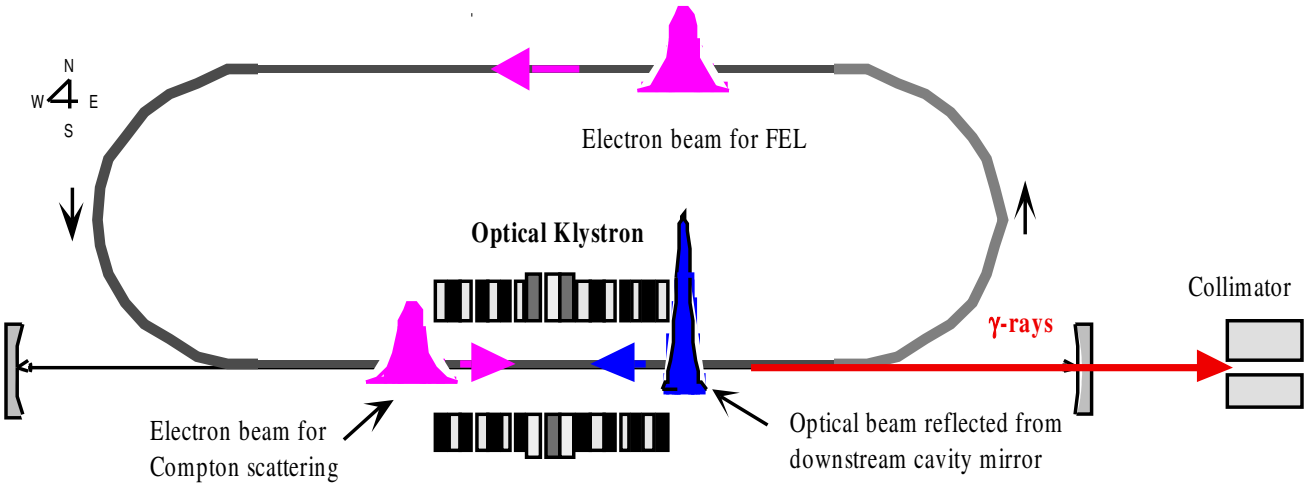

- **Two modes of operation:**
- No electron loss ($E_\gamma < 20$ MeV)
- Electron loss ($E_\gamma > 20$ MeV)

Upgraded Facility

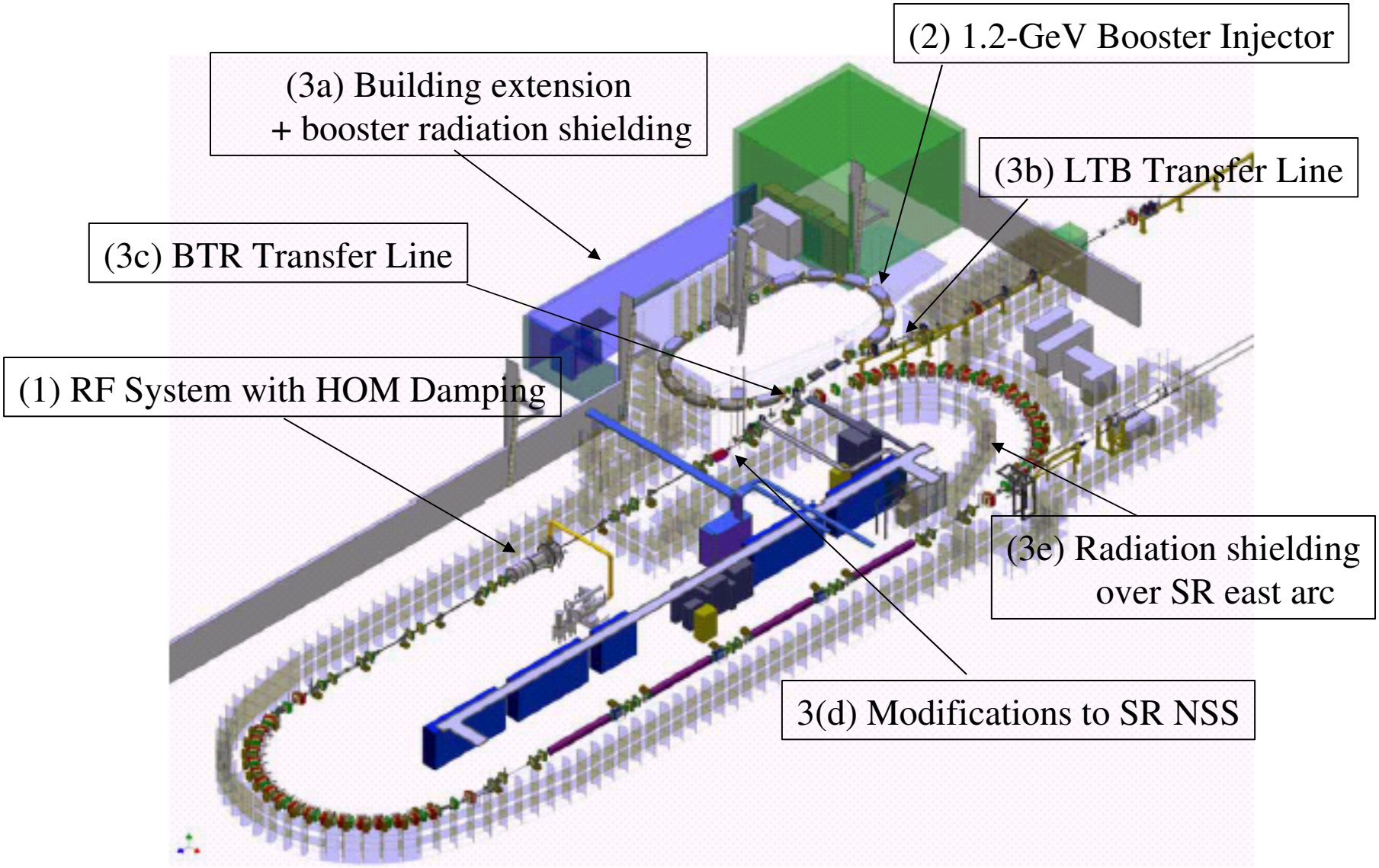

Ok-4 is a linear array, which produces linearly polarized beams.
Ok-5 is a helical wiggler which provides circularly polarized beams.

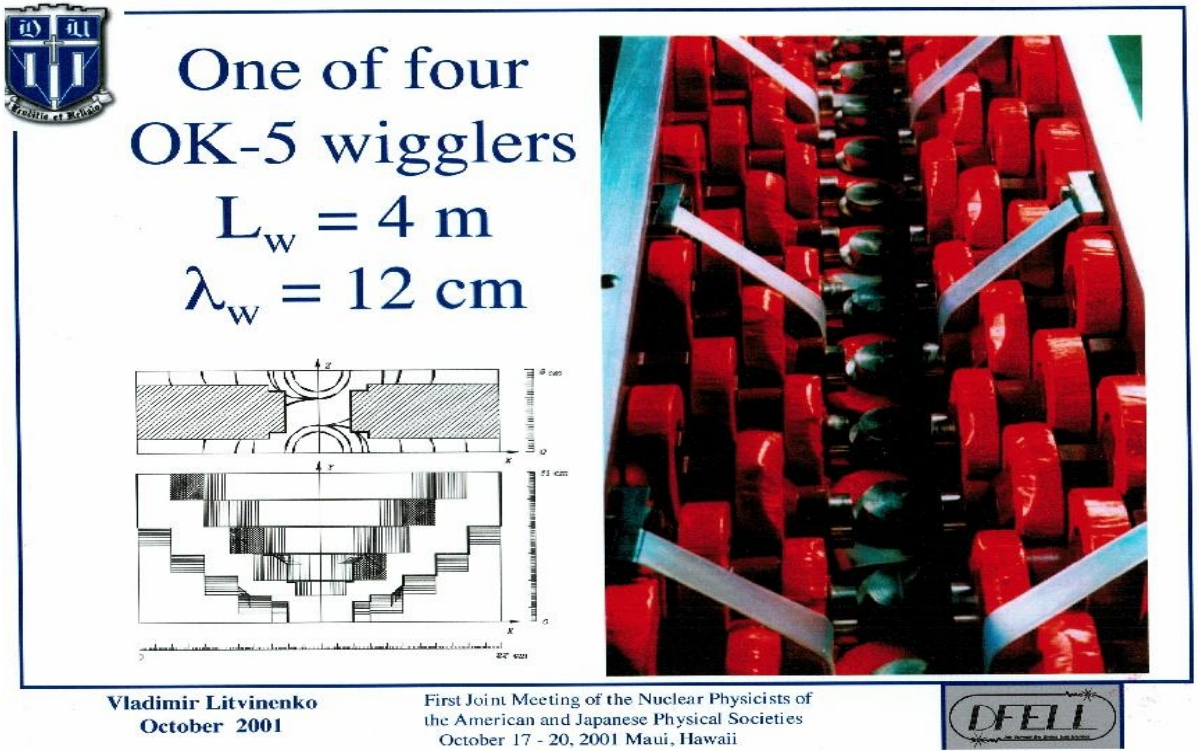

The FEL equation

The wavelength of the FEL photons in OK-4 is given by:

$$\lambda_{FEL} = \frac{\lambda_w}{2\gamma^2}\left[1 + \frac{K_w^2}{2}\right] \qquad \lambda_w = 10 \text{ cm}$$

K_w is called the wiggler parameter. It is varied by changing the magnetic field, is dimensionless, and varies between 0 and 5.4 for OK-4.

So the wavelength produced is varied by changing the magnetic field and the electron energy.

The 1.2 GeV Booster Injector

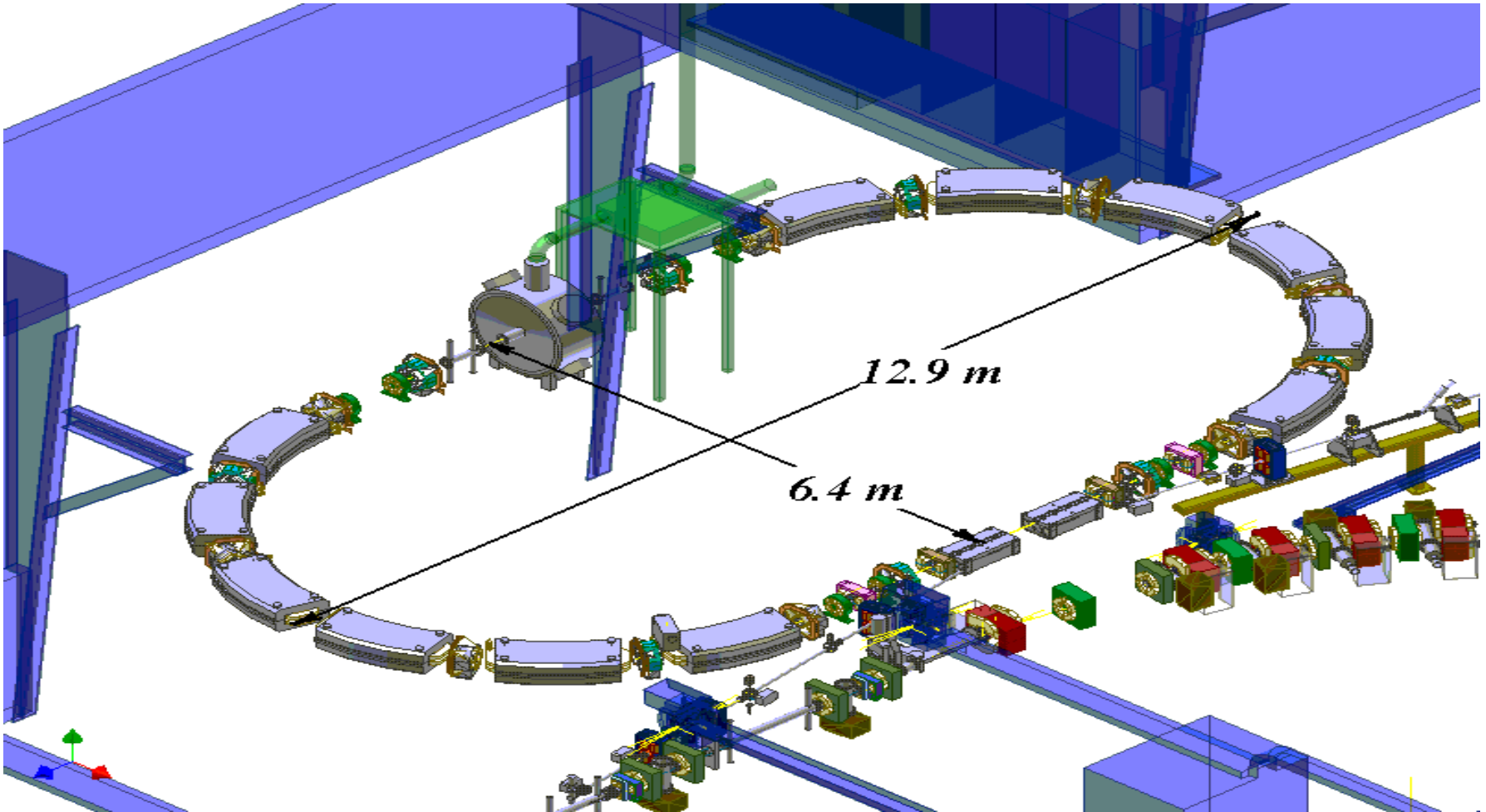

The Shielded Facility

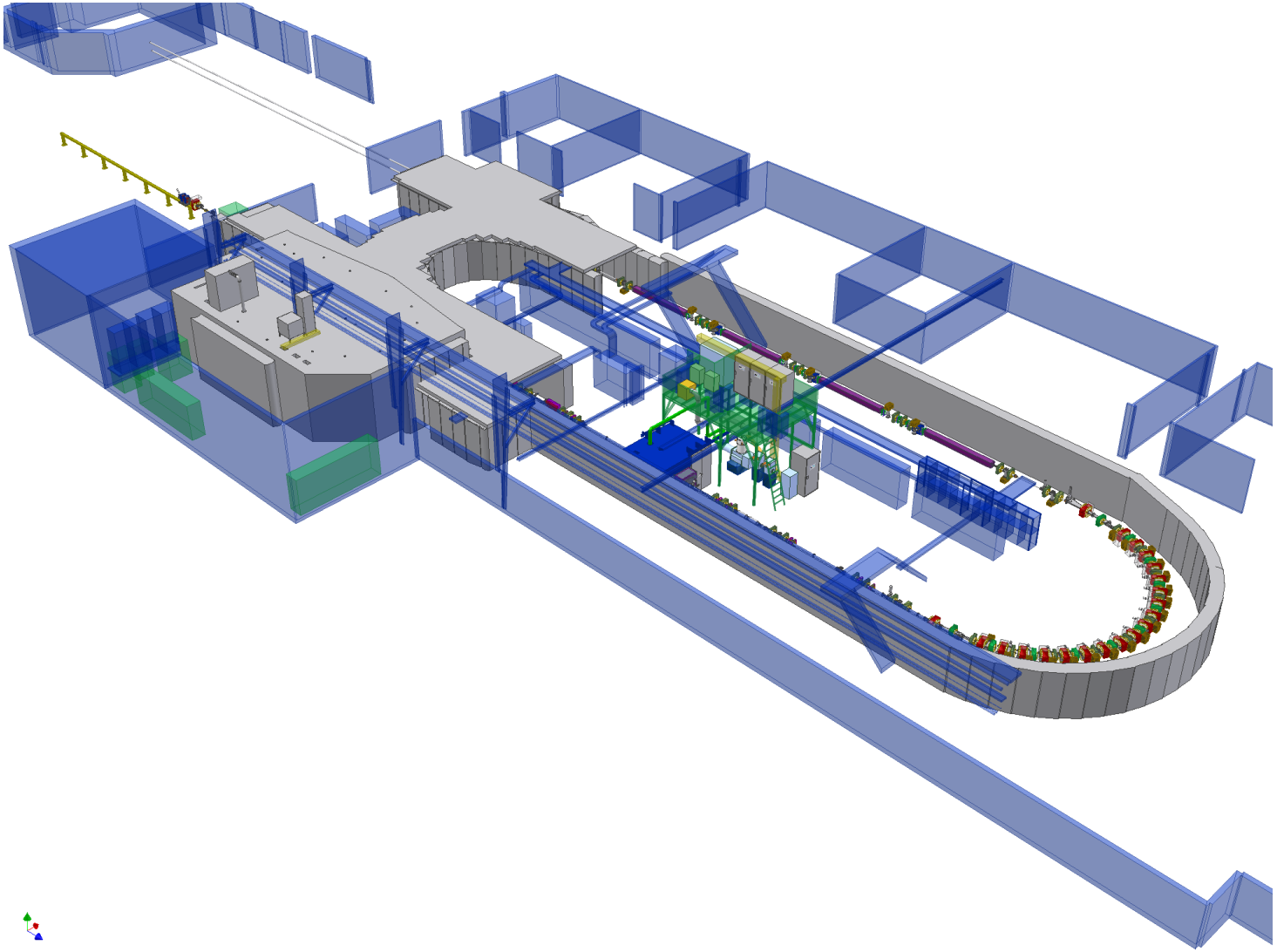

Compton backscattering

For a collision between a relativistic electron and a low E photon the energy of the scattered photons is peaked along the direction of the incident electrons with a max value at $\theta_f = 0$:

$$E_f = \frac{\gamma^2 (1 + \beta)^2}{1 + R_0} E_i$$

When the recoil term $R_0 = 2\gamma^2 (1 + \beta) E_i/E_e$ is small:

$$E_f \sim 4 \gamma^2 E_i$$

Ex.: *For a 1 GeV electron γ= 2000, so a 10 eV photon becomes a 160 MeV γ ray.*

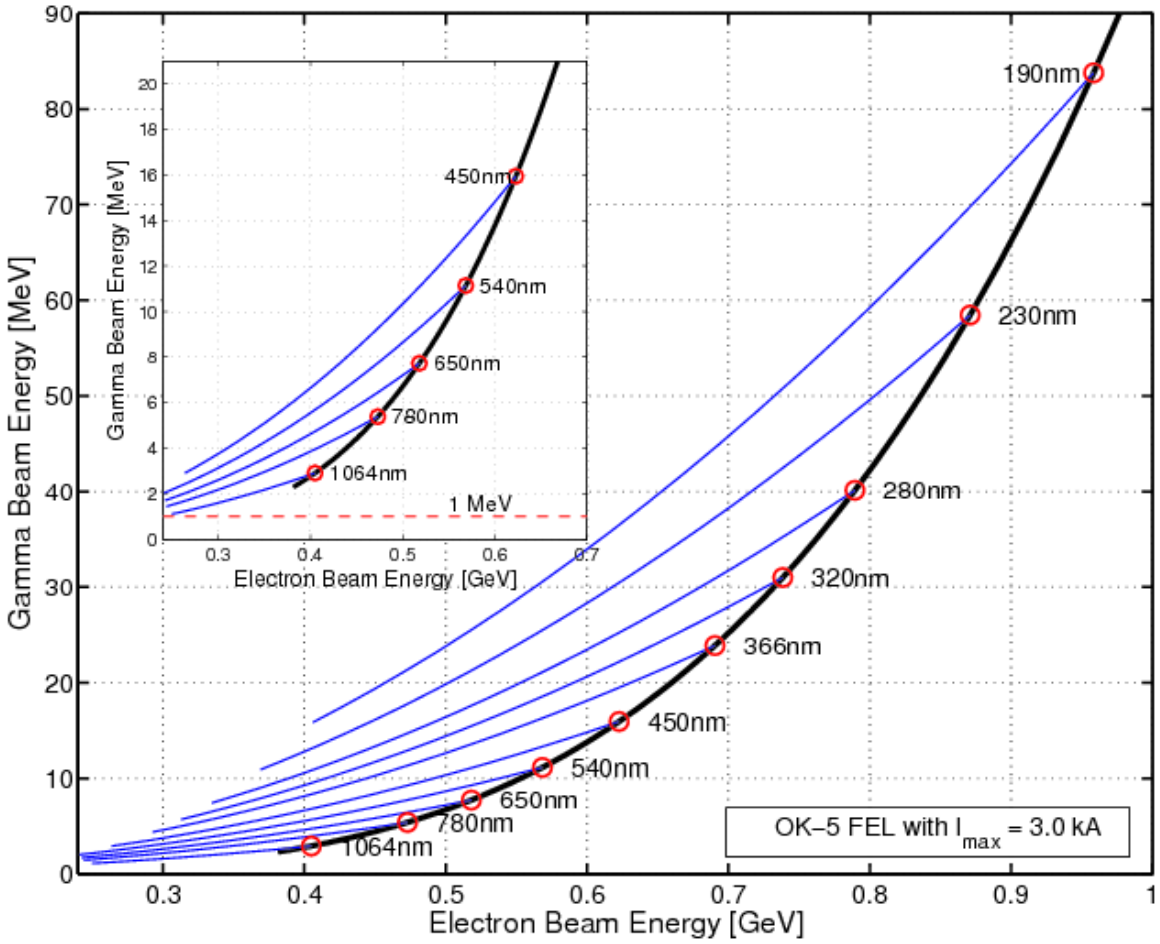

HUGS_1, June 2009

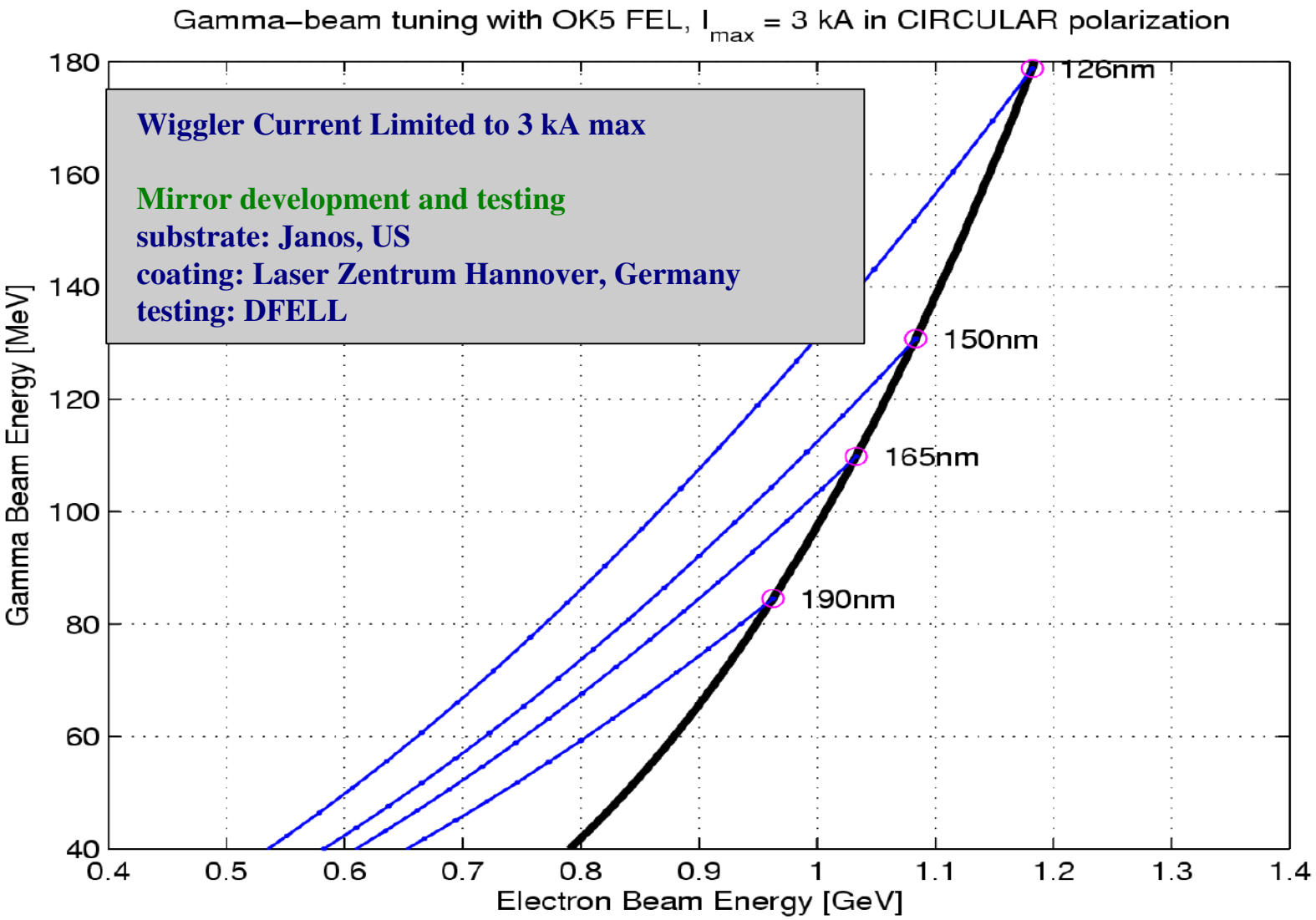
Gamma–beam tuning with OK5 FEL, I max = 3 kA in CIRCULAR polarization
Wiggler Current Limited to 3 kA max
Mirror development and testing
substrate: Janos, US
coating: Laser Zentrum Hannover, Germany
testing: DFELL
126nm
150nm
165nm
190nm
Gamma Beam Energy [MeV]
Electron Beam Energy [GeV]
180
160
140
120
100
80
60
40
0.4
0.5
0.6
0.7
0.8
0.9
1
1.1
1.2
1.3
1.4

Extending Gamma Energy Range (4 kA Wiggler Op)

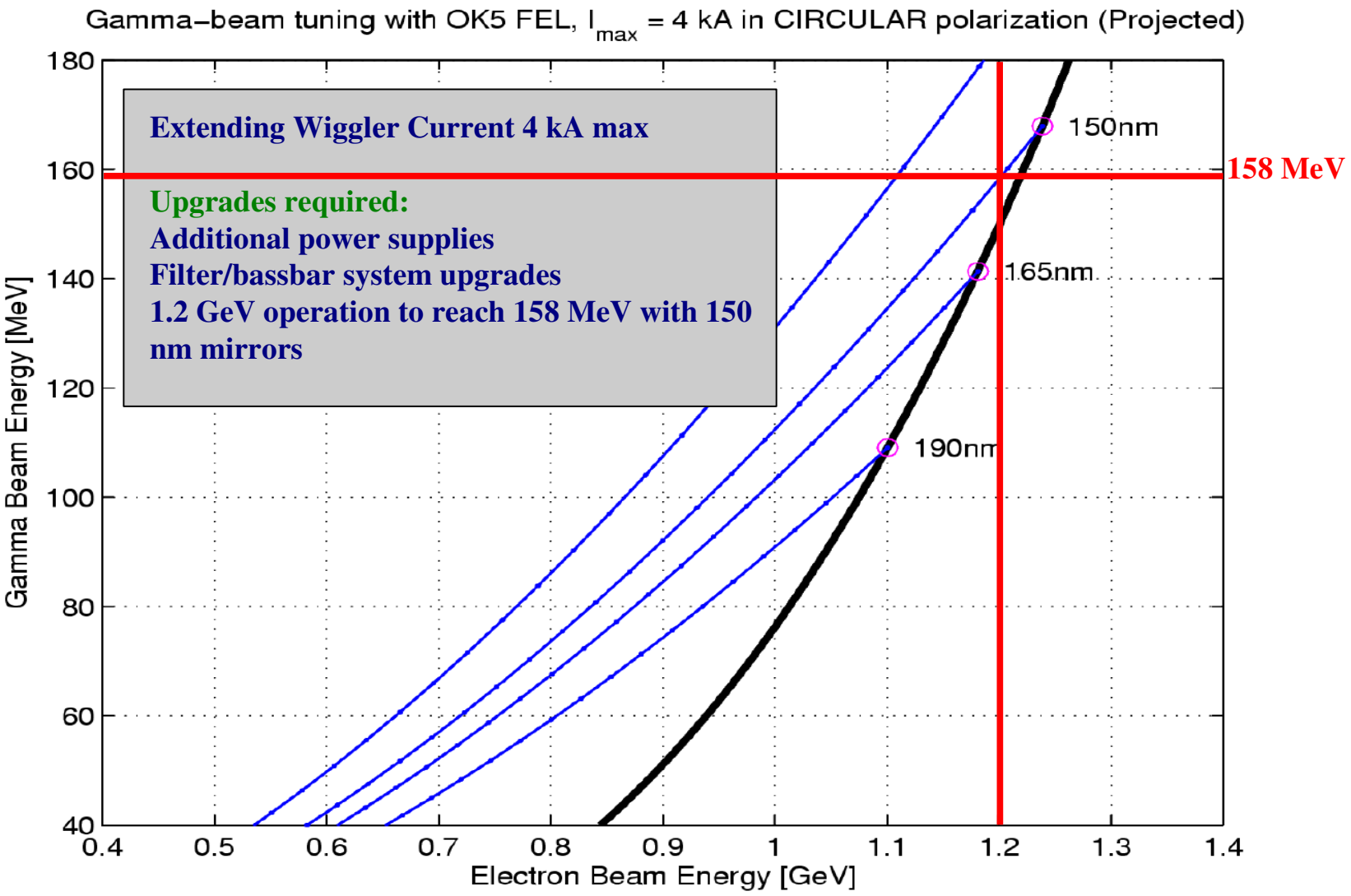

Some typical beam intensities

E_γ(MeV)	Beam on target ($\Delta E/E = 3\%$)
1 - 2	2×10^7 γ/s
8 – 16	8×10^7 (total flux of 2×10^9)
20 – 45	8×10^6
50 – 95	4×10^6 (by 2011)

•The research program at HIγS

•There is a very broad program of research underway at HIGS. This is expected to take over five years to execute, and will require over 2000 hrs. per year of beam time. The program includes:

- ***Nuclear Astrophysics***
- ***Few Body Physics***
- ***GDH Sum rule for deuterium and ^{3}He***
- ***Nuclear Structure studies using NRF***
- ***Compton scattering from nucleons and few body nuclei***
- ***Pion Threshold studies***

HIγS results

- ***Precision Data on photodisintegration of the Deuteron using 100% linearly polarized γ- rays near photodisintegration threshold.***

- ***Performed Nuclear Resonance Fluorescence measurements using the 100% linearly polarized γ- ray beam to make unambiguous parity assignments.***

- ***Compton scattering of polarized gamma rays from ^{16}O between 25 and 40 MeV.***

- ***2 and 3-body Photodisintegration of ^{3}He at 12.8 and 15 MeV using 100% linearly polarized gamma rays.***

Nuclear Structure@HIγS

- ***The HIγS Facility has advanced the method of NRF to a new level of precision and sensitivity.***

Utilize the 100% polarized beams at HIγS to study nuclear structure primarily by means of the technique of nuclear resonance fluorescence.

•***Understanding the nuclear dipole response, especially near particle emission threshold, is of broad current interest.***

•A knowledge of the dipole strength and mode (E1 vs M1) is important in understanding nuclear structure phenomena such as:

•

•***halo structures***
•***clustering***
•***local isospin resonances***
•***pygmy resonances***
•***proton-crust oscillations,***
•***dynamical M1 scissors mode,***
•**etc.**

•**Nuclear Resonance Fluorescence is a powerful means for studying the dipole strength in nuclei.**

•

•

•Nuclear Resonance Fluorescence-(NRF) Experiments at HIγS

•The analyzing power for dipole excitations in a nucleus with a 0^+ ground state is:

•

$\Sigma(90^0)$= **+1** for $J^\pi = 1^+$ **where** $\Sigma(90^0) = \frac{I(\phi = 0) - I(\phi = 90))}{I(\phi = 0) + I(\phi = 90)}$

-1 for $J^\pi = 1^-$

Four 60 % High purity Germanium detectors

Parity assignments to strong dipole excitations of ^{92}Zr and ^{96}Mo

(Phys Rev C70, 044317 (2004))

Crucial for identifying two-phonon excitations originating from inhomogeneous phonon coupling.

Confirmed the 3472 keV state in ^{92}Zr as the dominant fragment of the M1 excitation strength function.

Identified 3 strong M1 states in ^{96}Mo as fragments of the 1^+ member of the mixed-symmetry 2-phonon multiplet of this nucleus.

Example of an E1 and an M1 transition in ^{96}Mo

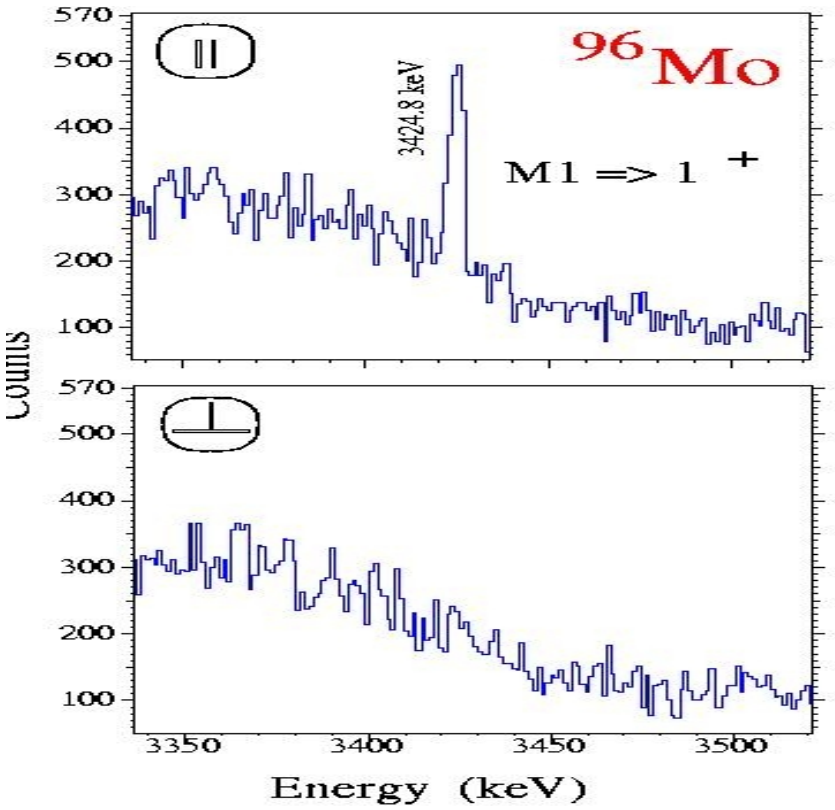

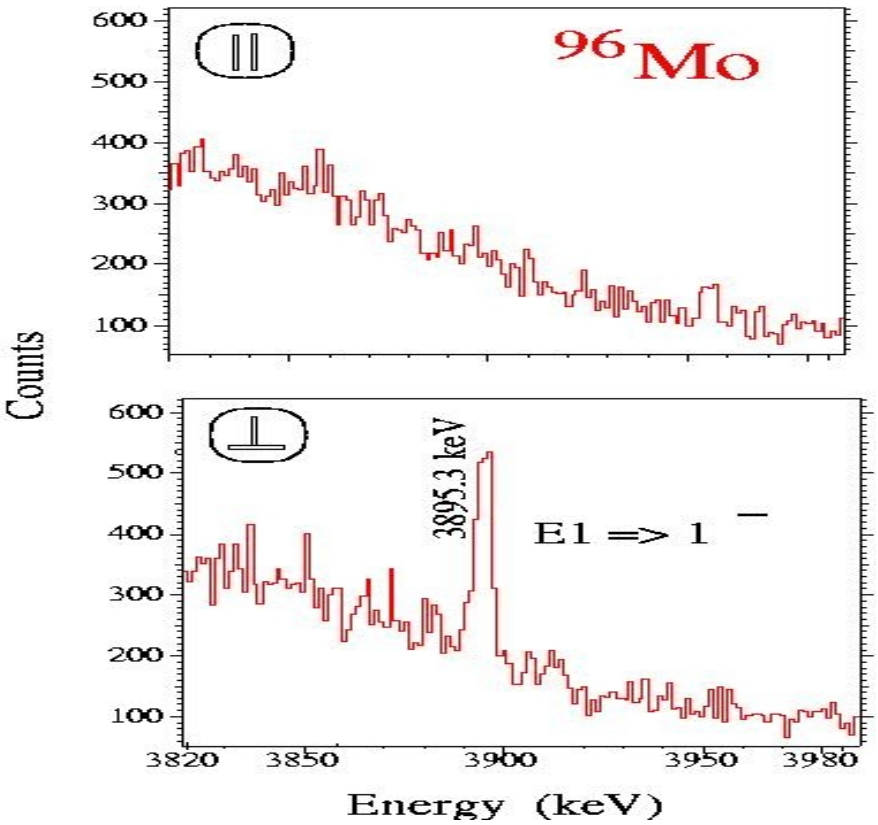

M1 Resonance Excitation in ^{92}Zr at 3471.7 keV

(Beam on target 5.5 hr)

Horizontal Vertical

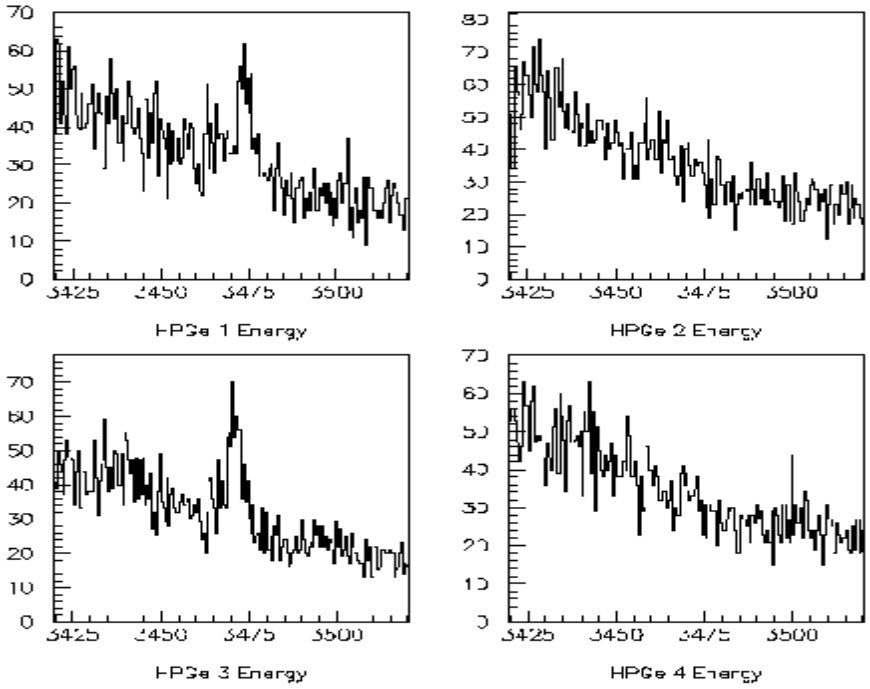

Recent result from NRF on ^{40}Ar

T.C. Li, N. Pietralla, G. Rainovski, A. Tonchev, H.R. Weller, M. Blackston, M.Ahmed,Y.Parpottas, B. Perdue, K. Keeter, C. Angel, J. Li, I.V. Pinayev, Y.Wu

Phys. Rev. C 73 (2006) 054306

The HIGS experiment identified 25 dipole states, finding one 1+ state at 9.757 MeV, with B(M1)=0.14(3) nm. (The target was a 4500 psi gas cell!)

Argon gas target: 4500 psi, 12 cm long→ 6.64 g/cm^2

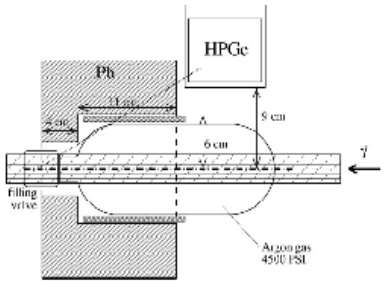

FIG. 1. Schematic cross section of the arrangement of the argon gas container and the HPGe γ-ray detectors (only one shown, see text).

γ-ray beam. The γ-ray flux on target amounted to about 1.0 photon/(eV s). The target consisted of natural argon gas (99.6% ^{40}Ar) pressurized to 4500 PSI. It was stored in a container consisting of an aluminum core wrapped in carbon fiber, which was placed along the beam axis. Its effective length was 12 cm, giving an effective target thickness of 6.64 g/cm^2. The target holder was a 5-cm-thick Pb ring which also shielded the downstream end of the container, including the filling valve made of brass, from the detectors. Figure 1 shows the cross section of the target setup, argon gas container supported by the target holder, and one of the four HPGe detectors.

The incident beam hit the target to produce scattered photons which were detected by four 60% relative efficiency HPGe detectors mounted at a distance of 9 cm from the beam axis in a polarimeter arrangement. The four detectors were positioned at a mean polar angle of $\bar{\theta} = 90°$ relative to the beam axis and at azimuthal angles of $\phi = 0°, 90°, 180°, 270°$ with respect to the horizontal polarization plane of the incident beam. Two detectors, at azimuthal angles $\phi_\parallel = \{0°, 180°\}$, measured in-plane photon scattering intensity along the polarization direction and the other two, at azimuthal angles $\phi_\perp = \{90°, 270°\}$, measured the out-of-plane intensity perpendicular to it. Data were taken for about 60 h at the above eight energies. The setup was energy calibrated before and after the experimental runs with a ^{11}B target placed at the original target position using an incident beam of $\bar{E}_\gamma = 8.9(3)$ MeV. The excited $\frac{5}{2}^-$ level at 8.92 MeV in ^{11}B and its single escape transition, as well as some background lines, provided good energy calibration points for the high energy range of this experiment, i.e., 7.7 to 11 MeV. For the low energy range, a ^{56}Co source was used for energy calibration up to 3.6 MeV. Relative efficiencies $r(E_\gamma) = \epsilon(\phi_\parallel)/\epsilon(\phi_\perp)$ of the detectors at azimuthal angles $\phi_\parallel, \phi_\perp$ was measured using the data from the ^{11}B and ^{56}Co runs. For example, $r = 0.90(20)$, $0.76(20)$ at $E_\gamma = 8.5$, 9.5 MeV, respectively. Figure 2 shows nuclear resonance fluorescence (NRF) spectra obtained at azimuthal angles $\phi_\parallel$ and $\phi_\perp$, and mean polar angle $\bar{\theta} = 90°$ from two beam energies $\bar{E}_\gamma = 8.6$ and 9.8 MeV. Peaks labeled with spin and parity quantum numbers represent ground state transitions.

The intensity distribution function derived within the angular correlation formalism [17,18] of a $0^+ \xrightarrow{\vec{\gamma}} 1^\pi \xrightarrow{\gamma} 0^+$

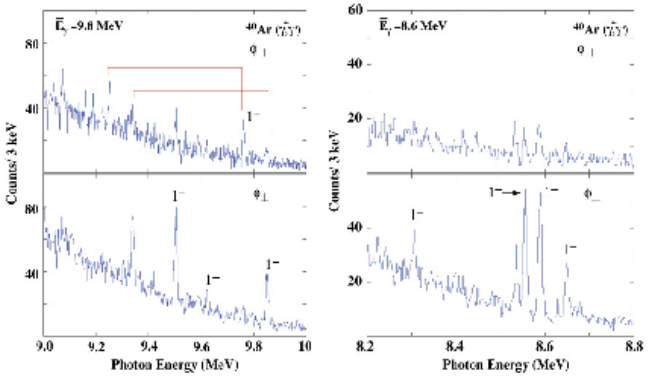

FIG. 2. (Color online) Spectra of the ^{40}Ar($\vec{\gamma}, \gamma'$) reaction at HIγS. Data were taken at a mean polar angle $\bar{\theta} = 90°$ relative to the incident photon beam and azimuthal angles $\phi_\parallel$ (top) and $\phi_\perp$ (bottom) relative to the polarization plane of the γ-ray beam. The mean γ-ray energy $\bar{E}_\gamma$ of the incident beam is given in the upper left corners. The J^π assignments are indicated for the ground state transitions in ^{40}Ar. The single escape peaks from some ground state transitions are indicated by brackets.

TABLE II. The excitation energy E_x, total magnetic dipole excitation strength $B(M1)\uparrow$ and strength contributed by the proton spin $B(M1_{\sigma_p})\uparrow$ for the first ten 1^+ states in ^{40}Ar obtained from shell model calculations as described in the text.

E_x (MeV)	$B(M1)\uparrow$ (μ_N^2)	$B(M1_{\sigma_p})\uparrow$ (μ_N^2)
4.692	0.428	0.011
5.377	0.031	0.024
6.882	0.197	0.440
8.081	0.005	0.011
8.279	0.015	0.004
9.465	0.107	0.105
9.937	0.005	0.008
10.420	0.036	0.038
11.263	0.007	0.006
12.044	0.004	0.002

1^+ states. For the $M1$ operator we have used a quenching factor of 0.7 for the spin g-factors, 1.1 for the proton orbital g-factor and 0.1 for the neutron orbital g-factor. Figure 5 displays the $M1$ strengths measured in the experiment along with the predictions of this calculation. On the top part, the cross-hatched areas are meant to indicate that the energy regions below 7.7 MeV and above 11 MeV were not investigated in this experiment. A lower limit for the detection of $M1$ strength of 0.05 μ_N^2 was estimated from Ref. [10] for energies between 7.7 and 11 MeV. Any $M1$ strength below this limit could not be detected and therefore this area is also cross-hatched in Fig. 4. The middle and bottom parts of the figure show the distribution of $M1$ strengths and compares the proton spin contribution to the total $B(M1)\uparrow$ for the ten predicted 1^+ states in ^{40}Ar. Among them, the third 1^+ state at 6.882 MeV has the largest proton spin contribution [$B(M1_{\sigma_p})\uparrow = 0.440\ \mu_N^2$] to the total $B(M1)\uparrow$. Unfortunately, the mirrors of the optical cavity at HIγS made it impossible at the time of the experiment to cover the energy range below 7.7 MeV and, hence, that dominant fragment of the $\pi(d_{5/2} \rightarrow d_{3/2})$ spin-flip strength could not be investigated. The other state which was dominated by the $\pi(d_{5/2} \rightarrow d_{3/2})$ spin-flip transition is the sixth 1^+ state at 9.465 MeV, which has the second largest proton spin contribution [$B(M1_{\sigma_p})\uparrow = 0.105\ \mu_N^2$] to the total $B(M1)\uparrow$. The excitation energies of this predicted 1^+ state at 9.465 MeV and our experimentally identified 1^+ state at 9.757 MeV are very close. The experimental magnetic dipole excitation strength $B(M1_{\text{exp}})\uparrow = 0.148(59)\ \mu_N^2$ agrees with $B(M1_{\text{theo}})\uparrow = 0.107\ \mu_N^2$ (see Table II) within uncertainties. Based on the excellent agreement of both their E_x and $B(M1)\uparrow$, we interpret the origin of our experimentally identified 1^+ state at 9.757 MeV as one fragment of the proton $d_{5/2} \rightarrow d_{3/2}$ spin-flip transition in ^{40}Ar at that excitation energy. Despite the fact that this is only a small part of the total $d_{5/2} \rightarrow d_{3/2}$ proton spin-flip strength (total = 2 μ_N^2, expected), present experimental results supported by the shell model prediction indicate that the proton spin-flip strength is not fully concentrated in the energy interval between 8 and 11 MeV. A similar situation has been observed for ^{36}Ar and ^{38}Ar [21] where the $M1$ strength is even more

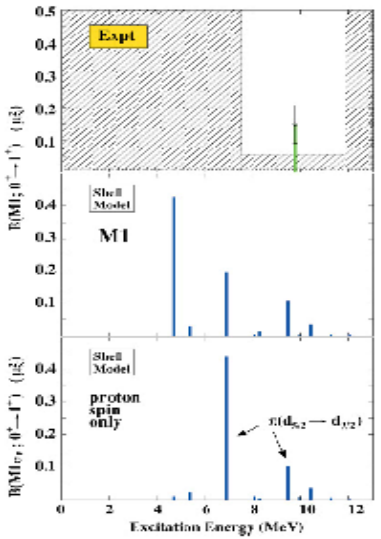

FIG. 5. (Color online) Experimental and theoretical $M1$ strength distributions in ^{40}Ar. (top) The single known 1^+ state observed here at 9.757 MeV within an energy region between 7.7 and 11 MeV. Other energy and strength regions, to which our experiment was insensitive, are shaded. The distribution of the magnetic dipole excitation strengths $B(M1)\uparrow$ (middle) and the proton spin contribution $B(M1_{\sigma_p})\uparrow$ (bottom) of the first ten 1^+ states predicted by the shell model calculation. Proton $d_{5/2} \rightarrow d_{3/2}$ spin-flip transition strength dominates the $M1$ matrix elements for the third and sixth 1^+ states at 6.882 and 9.465 MeV, respectively, as labeled.

smoothly distributed between 6 and 15 MeV. To gain deeper insight into the structure of argon isotopes near neutron number $N = 20$ and to reveal the role of multiparticle-multihole excitations across the $N = 20$ shell closure it is necessary to investigate experimentally whether the strength in neutron-rich argon isotopes is distributed according to the present shell model picture for ^{40}Ar (Fig. 5, middle and bottom), which shows no cross-shell excitations, or whether it is even more strongly fragmented as in the case of ^{38}Ar.

V. SUMMARY

^{40}Ar($\vec{\gamma}, \gamma'$) photon scattering experiments have been performed using the nearly monochromatic, linearly polarized photon beam of HIγS. Eight beam energy settings have been used to cover the energy range from 7.7 to 11 MeV. 28 dipole excitations within this range were observed and their parity quantum numbers were unambiguously assigned from the azimuthal intensity asymmetry of nuclear resonance

A shell model calculation predicts that the proton $d_{5/2}$ -> $d_{3/2}$ spin-flip transition strength dominates the M1 matrix elements for the states at 6.882 (0.44 μ_N^2) and 9.465 MeV (0.105 μ_N^2) .

The 1^+ state observed at 9.757 MeV (0.148(59) μ_N^2) is identified as the first spin-flip M1 strength observed in ^{40}Ar.

Collaborative Research: Nuclear Data Measurements using HIGS

Domestic Nuclear Detection Office (DNDO)/NSF Proposal:

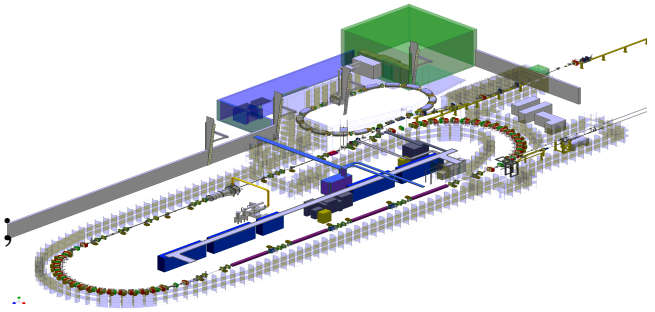

- Search for low-spin states in ^{235,238}U, ^{239}Pu, and ^{241}Am; *important for developing technologies to scan cargo containers*
- Gamma-ray attenuation coefficients at 3 to 50 MeV; *important for improving image reconstruction*
- Development of instrumentation for (γ ,n) and (γ ,f) cross section measurements

Broader Aspect

- Support 100 hours/yr of beam time at HIGS
- Several graduate and undergraduate students

Team: C.R. Howell, A. Tonchev, W. Tornow (Duke), H.J. Karwowski (UNC), and R.S. Pedroni (NC A&T); Proposal numbers: 0736155/0736123/0736119

NRF Setup at HIGS

This project takes full advantage of the upgraded HIGS facility and cutting-edge gamma-ray detection system

Gamma beam: $\Phi_\gamma > 10^8$ γ/s (100 γ/s/eV), FWHM=3%, pulsed and polarized

Detector system: 4 Clovers + BGO; $\varepsilon_{array} = 1.4\%$ @ $E_\gamma = 1.33$ MeV

NRF Capabilities at HIGS: Excitation energies E_x; spin and parities J, π; branching ratio Γ_f / Γ_0 ground state widths Γ_0

In completely model independent way !

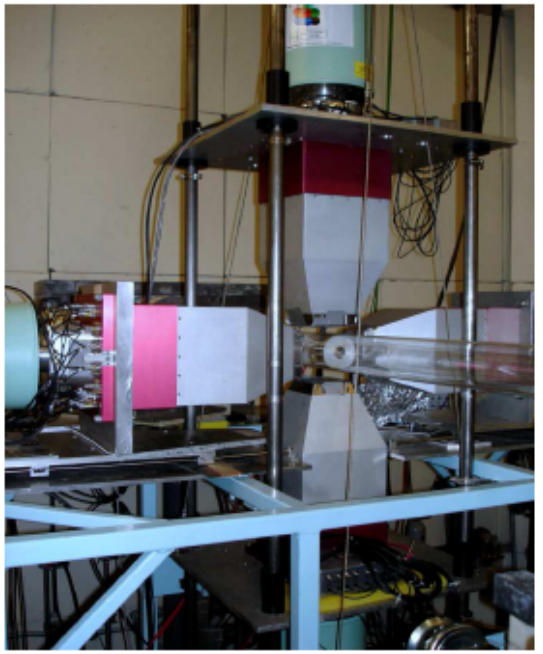

Clover Quartet

HIGS: Pushing the Limit of Sensitivity

$^{138}Ba(\gamma,\gamma')$ $E_\gamma = 5.40$ MeV

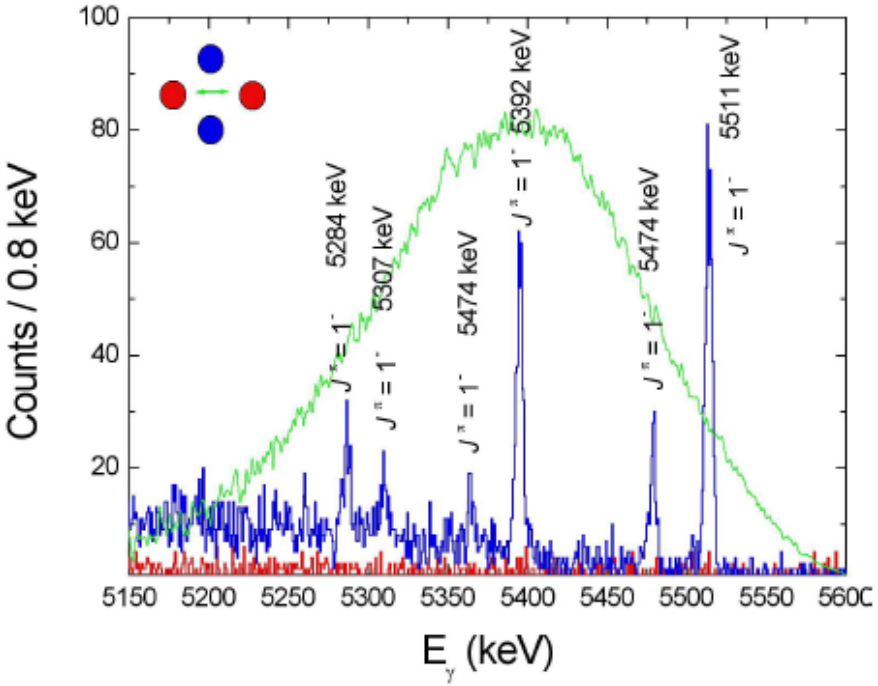

High detection sensitivities: resonance states with $\Gamma_{tot} \geq 1$meV

Dennis McNabb et al. (LLNL) tested the *FINDER concept using HIγS* beams (T-REX will use terawatt lasers to produce ~2 MeV γs with intensities of 10^6/eV/s.)

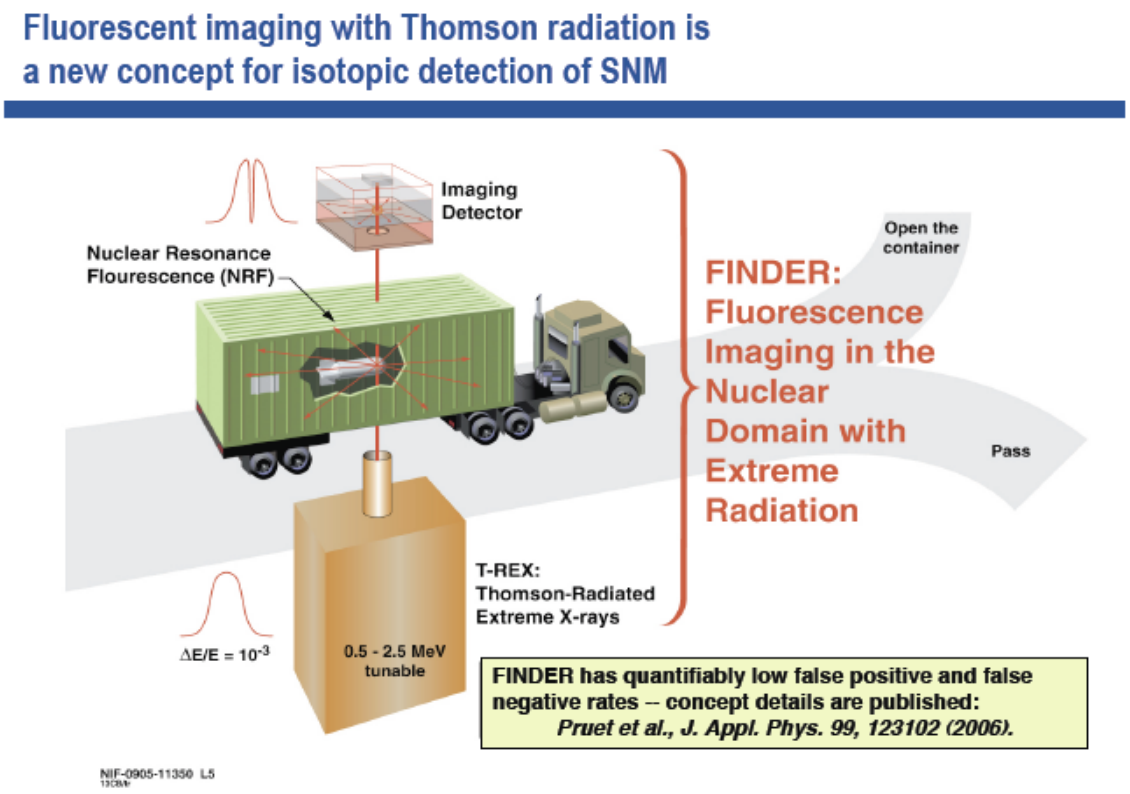

- **Basic idea:**
- Use an array of detectors to measure the rate of resonant scattering within a sample to determine the flux of resonance photons exiting the cargo.

- Measure the flux of off-resonant photons with a transmission detector placed in the beam.

- ***A disparity between the attenuation suffered by resonant and off-resonant photons indicates the presence of the material.***

J. Appl. Phys. **99**, 123102 (2006)

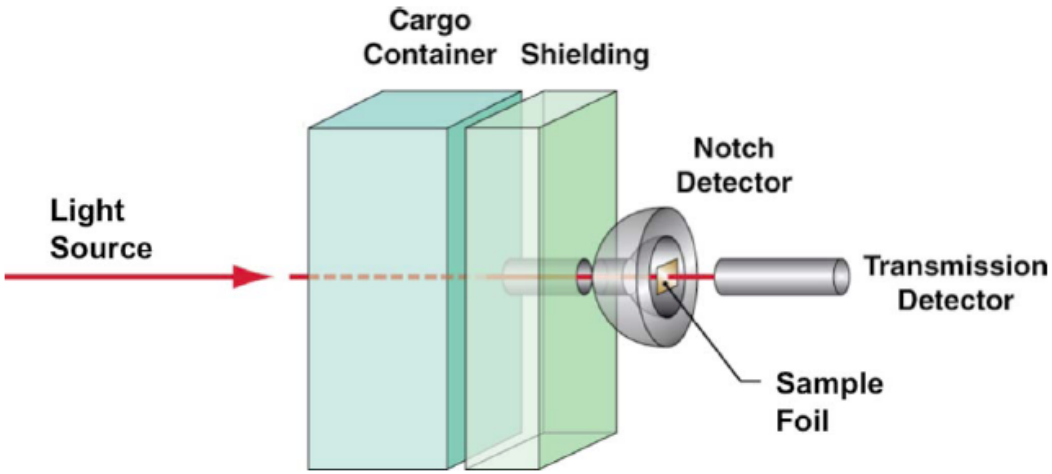

FIG. 2. (Color online) Schematic representation of the detection system studied here. A photon beam is sent to interrogation cargo. After passing through the container the flux of resonant and off-resonant photons is measured. Resonant flux is measured by "notch detectors" that observe NRF within a small sample foil made of the isotope that is being looked for. The flux of off-resonant photons is measured with a simple transmission or current detector.

Nuclear Astrophysics @HIγS

- Use the intense-low energy γ beams in order to perform precision measurements of key capture cross sections using the inverse reaction process.

•The $^{16}O(\gamma,\alpha)^{12}C$ reaction at HIγS

•The inverse of the $^{12}C(\alpha,\gamma)^{16}O$ capture reaction, termed the *holy grail of nuclear astrophysics* by Willie Fowler.

•The ratio of carbon to oxygen at the end of helium burning is **crucial for understanding the fate of Type II Supernovae** and the **nucleosynthesis of heavy elements.**

•An oxygen rich star is predicted to end up as a **black hole**, while a carbon rich star leads to **neutron star**. And a minor change in the S-factor of the $^{12}C(\alpha,\gamma)^{16}O$ capture reaction (from 170 to 200 keV-b) can make all the difference.

•

Oxygen formation in stellar helium burning

C and O are produced during helium burning in Red Giant stars which then either undergo supernova explosion or collapse into a white dwarf.

The first stage in helium burning proceeds via the triple-alpha capture reaction: $^{8}Be(\alpha,\gamma)^{12}C$.

The formation of O then proceed via the $^{12}C(\alpha,\gamma)^{16}O$ reaction.

The cross section for this reaction at the Gamov-peak of ~300 keV is really important and determines the C/O ratio.

The C/O ratio at the end of helium burning determines, for example, whether a star that undergoes type II supernovae collapses into a black hole (O-rich) or a neutron star (C-rich).

The astrophysical S-factor

The rapid variation of cross section with energy is primarily due to the coulomb barrier. This makes it convenient to take the barrier penetration factor out of the cross section. So we define the S-factor, which is almost a constant at very low energies:

$$S = E \times \sigma \, e^{2\pi\eta}$$

where η is the Sommerfeld parameter ($Z_1 Z_2 \, \alpha/\beta$, where α is the fine structure constant and $\beta = v/c$) and σ is the cross section.

S-factors for CTAG

This reaction is dominated by two amplitudes at low energies corresponding to E1 and E2 absorption. E1 comes from p-wave capture, while E2 is the result of d-wave capture.

Since we have to extrapolate to 300 keV, both must be determined, since they will have different E-dependence and extrapolate differently.

Need to ultimately know them at the 10-20% level at 300 keV.

3.4. 25 $M_\odot$, a representative case

Figure 1 shows the effect of varying the $^{12}C(\alpha,\gamma)^{16}O$ rate on the presupernova profiles of the mass fractions of ^{16}O, ^{20}Ne, and ^{28}Si for the representative case of a 25 $M_\odot$ star with nominal semiconvection. In general, the oxygen abundance increases with the $^{12}C(\alpha,\gamma)^{16}O$ rate as expected, with the striking exception of the case where the rate is multiplied by 3.0. In that case, the shallower entropy gradients and barriers existing in the star have permitted a convective burning shell to extend outward to encompass most of the oxygen core, resulting in the burning of about half of the oxygen to silicon and sulfur. So little neon is produced in this star (owing to lack of carbon fuel) that the entropy jump at the neon-burning shell, that usually constrains the growth of the underlying oxygen-burning shell (e.g. see figs. 2a and 3 at an interior mass coordinate of 2.8 $M_\odot$), almost vanishes. The remaining entropy jump is then overwhelmed by the entropy generated by the progressively higher temperature, shell-oxygen burning that occurs as the star enters its

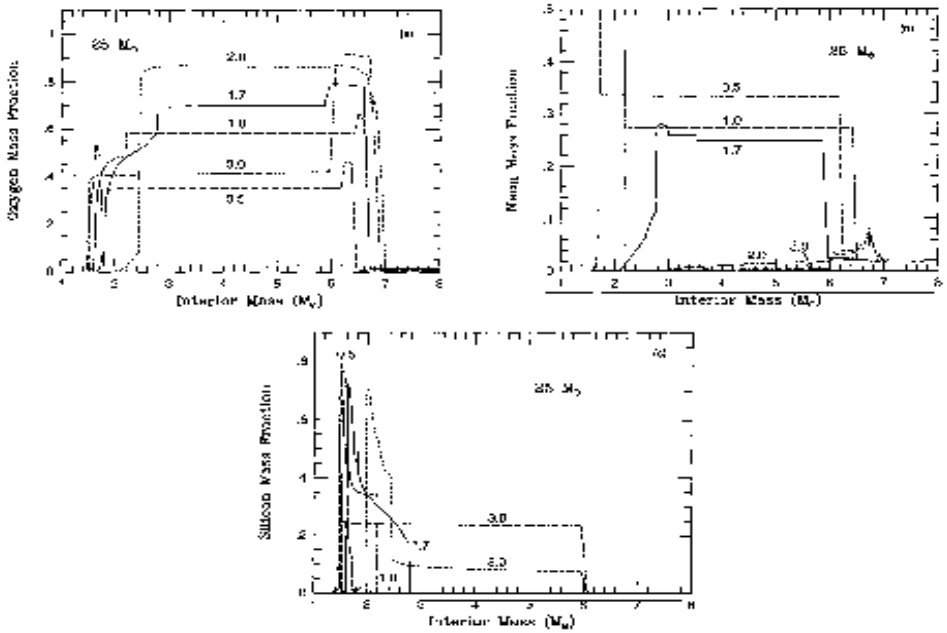

Fig. 1. Distribution of (a) ^{16}O, (b) ^{20}Ne, and (c) ^{28}Si with mass within the cores of five 25 $M_\odot$ stars calculated assuming a "nominal" amount of semiconvection ("S" series). Each curve is labelled with the multiple of the $^{12}C(\alpha,\gamma)^{16}O$ rate (CF88 = 1) used in its calculation and only the inner 8 $M_\odot$ of each star is shown. In general, increasing the α-capture rate on ^{12}C leads to an increase of oxygen production and a decrease in neon production for obvious reasons (neon is a carbon byproduct and thus reflects a smaller synthesis of carbon by helium burning). A less previous manifestation of the large reaction rate (and oxygen abundance) is an extensive convective oxygen-burning shell in which silicon is produced and the s-process destroyed.

World data on the $^{12}C(\alpha,\gamma)^{16}O$ cross section

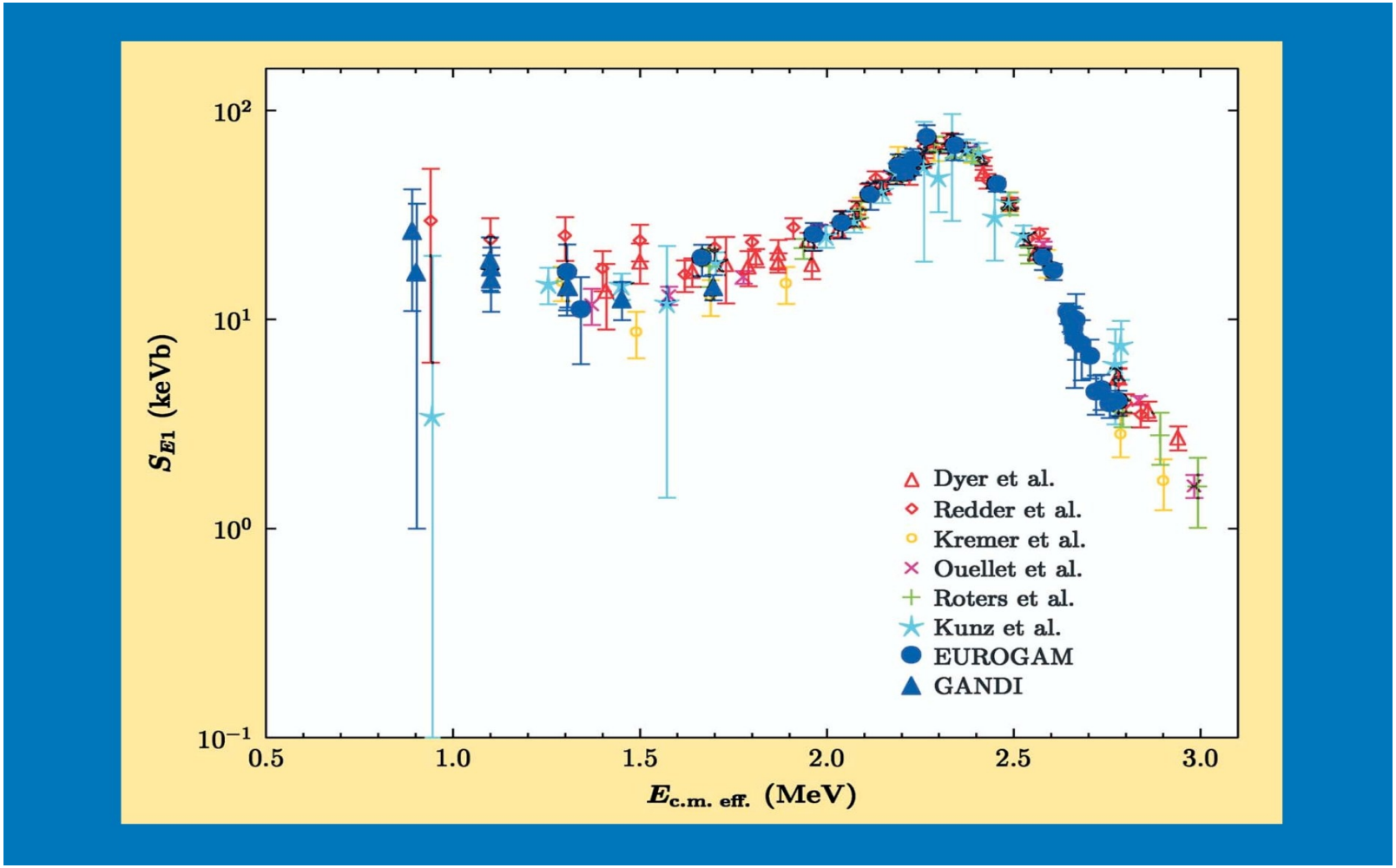

Results of the 3 most recent experiments were analyzed using R-Matrix theory to extrapolate to 300 keV. The resulting S-factor was assigned an uncertainty of +/-25%.
J.W. Hammer *et al.*, Nucl. Phys. A752, 514c(2005).

Extrapolation values S_{E1}^{300} and S_{E2}^{300} for the different combination of data sets A, B, and C (A = EUROGAM, B = GANDI, C = Kunz *et al.*). For all cases also data of elastic scattering [12–14] and ^{16}N decay [20,21] were considered. The result of case A + B + C yields the lowest uncertainty and is used for the calculation of the reaction rate.

Data from:	A	B	C	A + B	B + C	A + B + C
S_{E1}^{300} (keV b)	81 (20)	77 (19)	76 (20)	77 (19)	76 (18)	77 (17)
S_{E2}^{300} (keV b)	80 (27)	78 (26)	85 (30)	80 (25)	81 (23)	81 (22)
S_{tot}^{300} (keV b)	—	—	165 (50)	—	—	162 (39)

•Motivation for the $^{16}O(\gamma,\alpha)^{12}C$ experiment

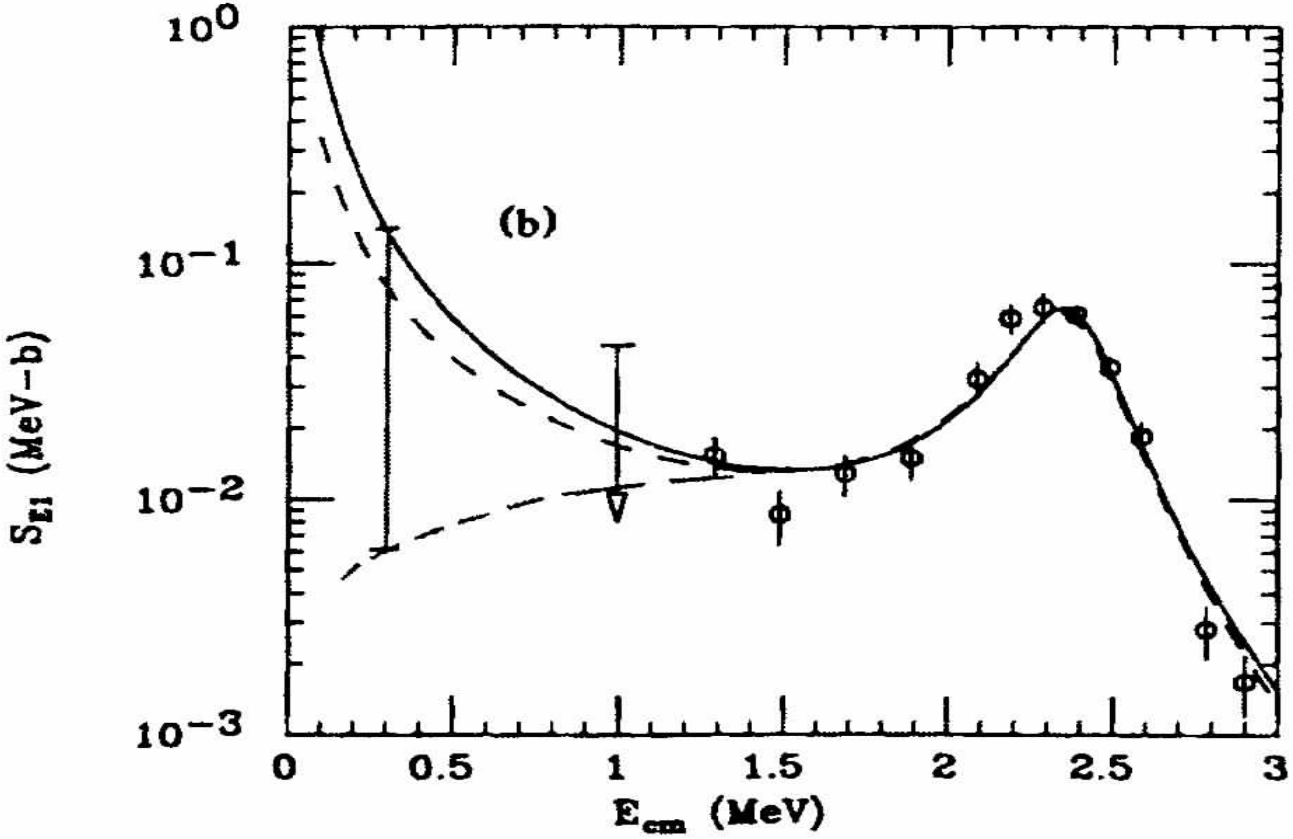

•CTAG@HIγS

•Measurement of the $^{16}O(\gamma,\alpha)^{12}C$ reaction at and below $E_\alpha(cm) = 2.6$ MeV. (Co-spokesperson: Dr. Moshe Gai.)

•*An optical readout Time Projection Chamber (TPC) has been constructed (Collaboration with UConn, Physikalisch Technische Bundesanstalt, Braunschweig, Germany and Weizmann Institute, Israel).*

•*This one-meter long high-resolution (2%) TPC allows for simultaneous detection of α's and ^{12}C's. Uses $N_2 + CO_2$ admixture for the scintillating gas.*

- Why use a gas filled TPC? The target is the detector. "Good" events will be unambiguous since both the outgoing α and ^{12}C tracks will be observed. Background free.

- Why an Optical TPC?

- 1. ***Cost*** is an order of magnitude less than conventional electronic readout TPC.
- 2. Easy data handling.
- 3. Reduced electronic noise--decoupled HV from readout electronics.
- 4. Improved reliability.
- 5. Well suited for Low Count Rate experiment.

•Schematic diagram of the Optical Time Projection Chamber @ HIγS (a UConn, PTB, Weizmann, Duke collaboration)

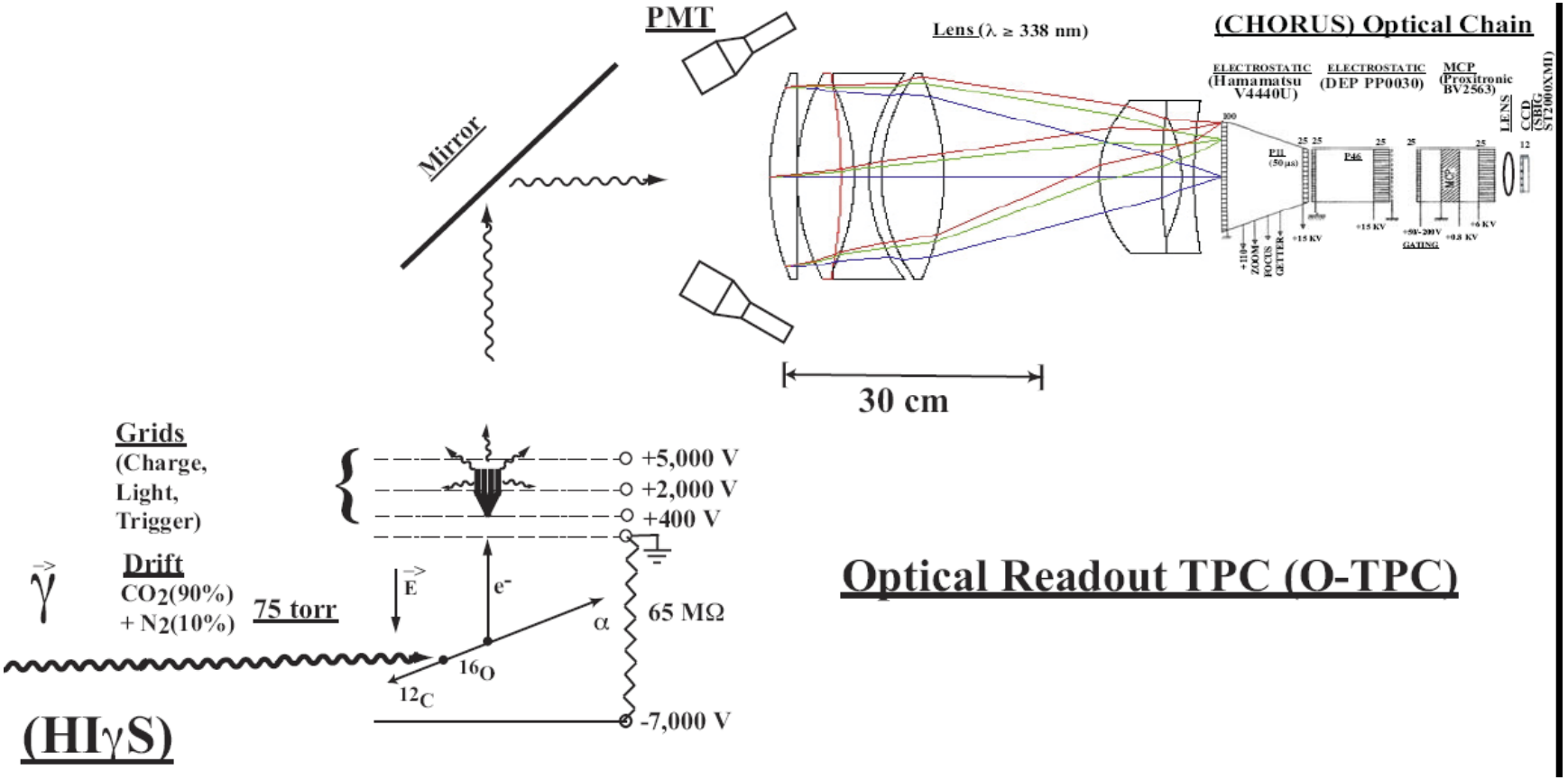

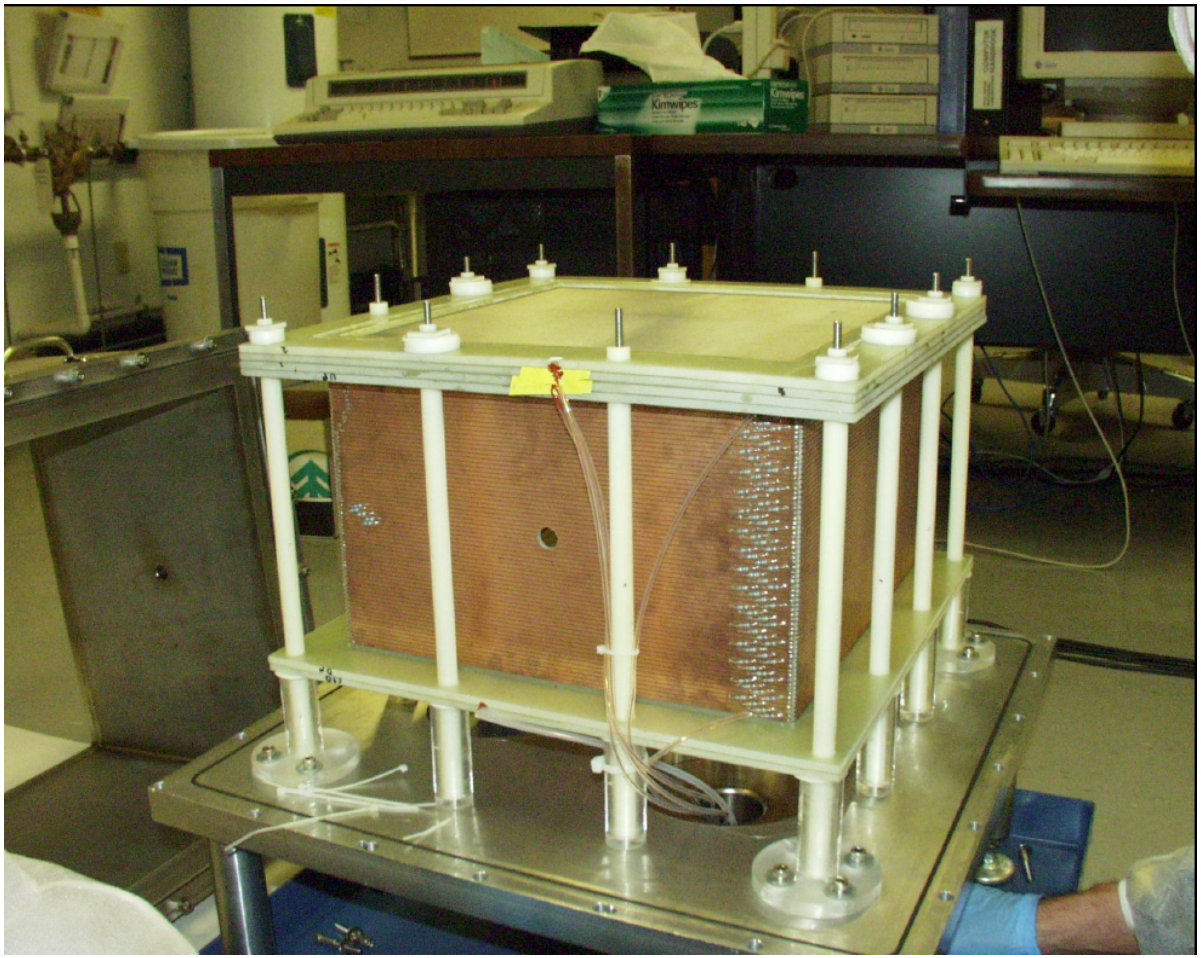

HUGS_1, June 2009

PTB
PTB

UCONN

•Tracks from 3.18 MeV alphas (^{148}Gd collimated source)

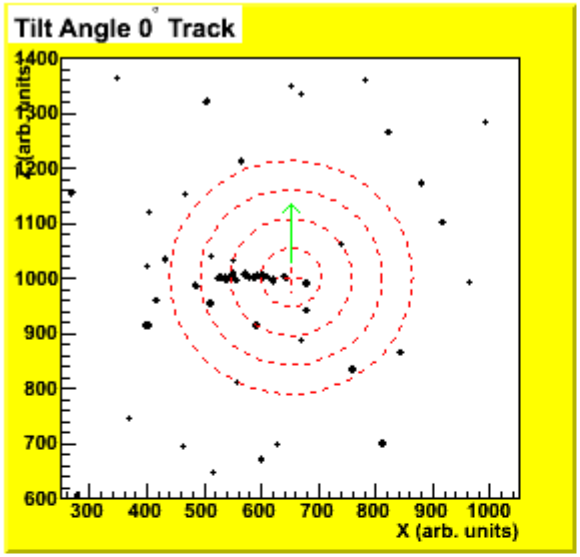

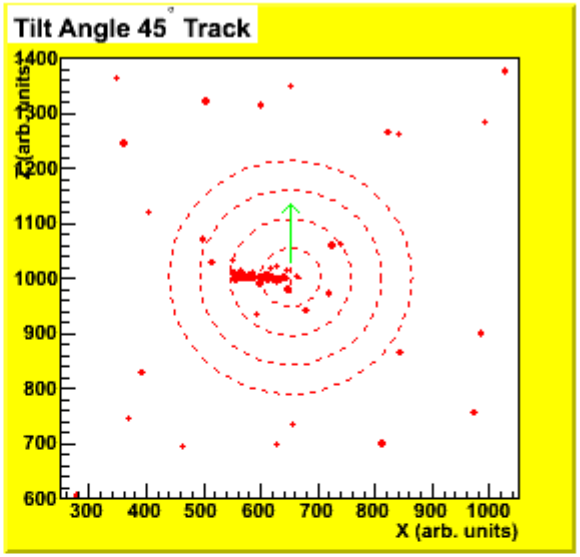

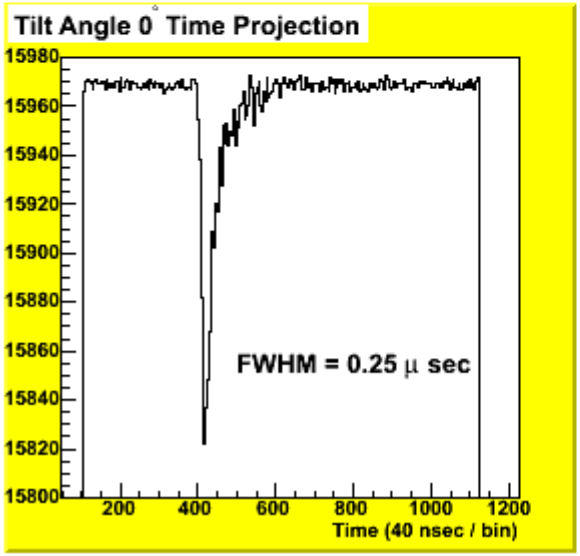

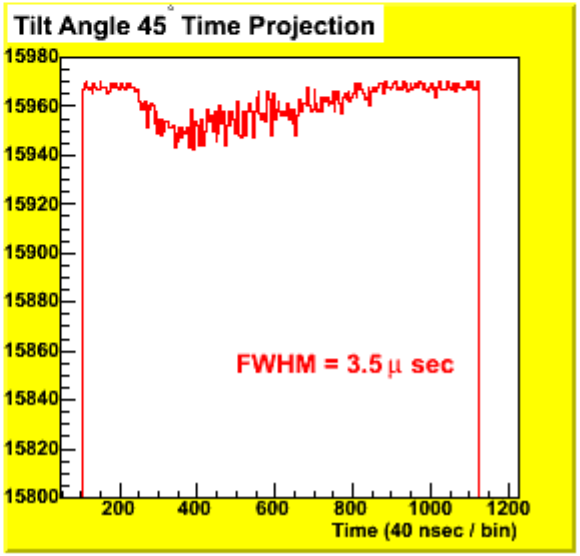

•The TPC will provide a target thickness of ~10^{20} nuc/cm^2 operating at 100 Torr. A beam intensity of 9 x 10^7 will require the following running times to obtain *10% accuracy for both the E1 and the E2 S-factors.*

•(Note: Data will be binned into 7 angular bins, with about 1000 counts per angular distribution.)

•**Ecm**	**E_γ(MeV)**	**Y(cph)**	**Time**
2.58	9.68	133	6 hrs
2.07	9.23	37	32 hrs
1.82	8.98	8	120 hrs
1.57	8.7	3	300 hrs

•Best measurements to date are Kunz et al. (PRL 86,3244(2001)) which achieved 30% uncertainties.
•The three most recent capture measurements invested almost 8000 hrs. of beam time. Even so, their results for S(E2) disagree by a factor of ~2.5!

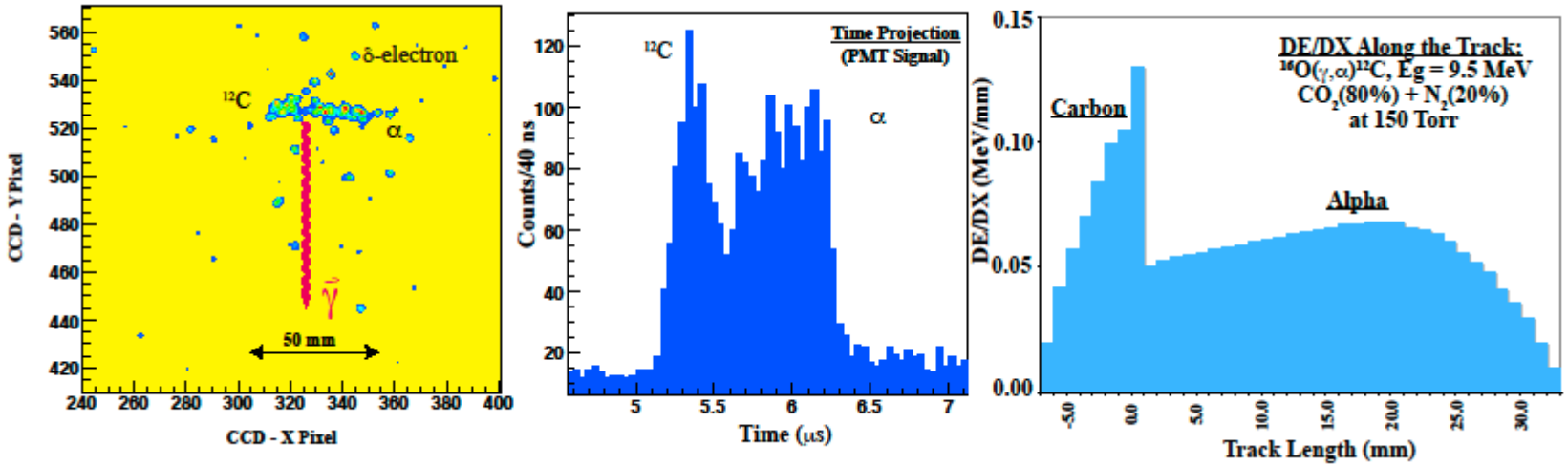
δ-electron
^{12}C
α
γ
50 mm
CCD - Y Pixel
CCD - X Pixel
Time Projection
(PMT Signal)
^{12}C
α
Counts/40 ns
Time (μs)
DE/DX Along the Track:
^{16}O(γ,α)^{12}C, Eg = 9.5 MeV
CO_2(80%) + N_2(20%)
at 150 Torr
Carbon
Alpha
DE/DX (MeV/mm)
Track Length (mm)

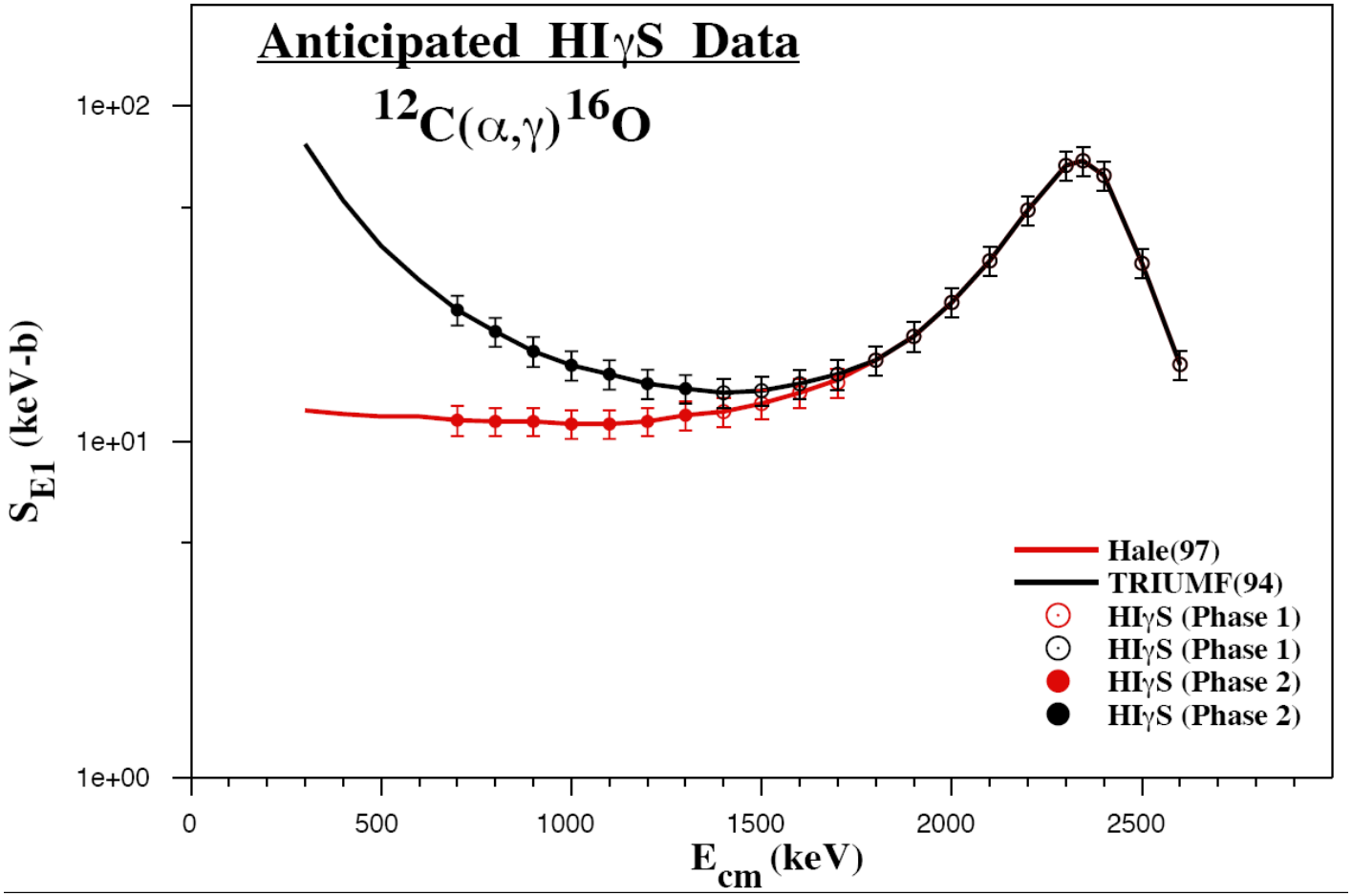
Anticipated HIγS Data
$^{12}C(\alpha,\gamma)^{16}O$
1e+02
1e+01
1e+00
S_{E1} (keV-b)
0
500
1000
1500
2000
2500
E_{cm} (keV)
Hale(97)
TRIUMF(94)
HIγS (Phase 1)
HIγS (Phase 1)
HIγS (Phase 2)
HIγS (Phase 2)

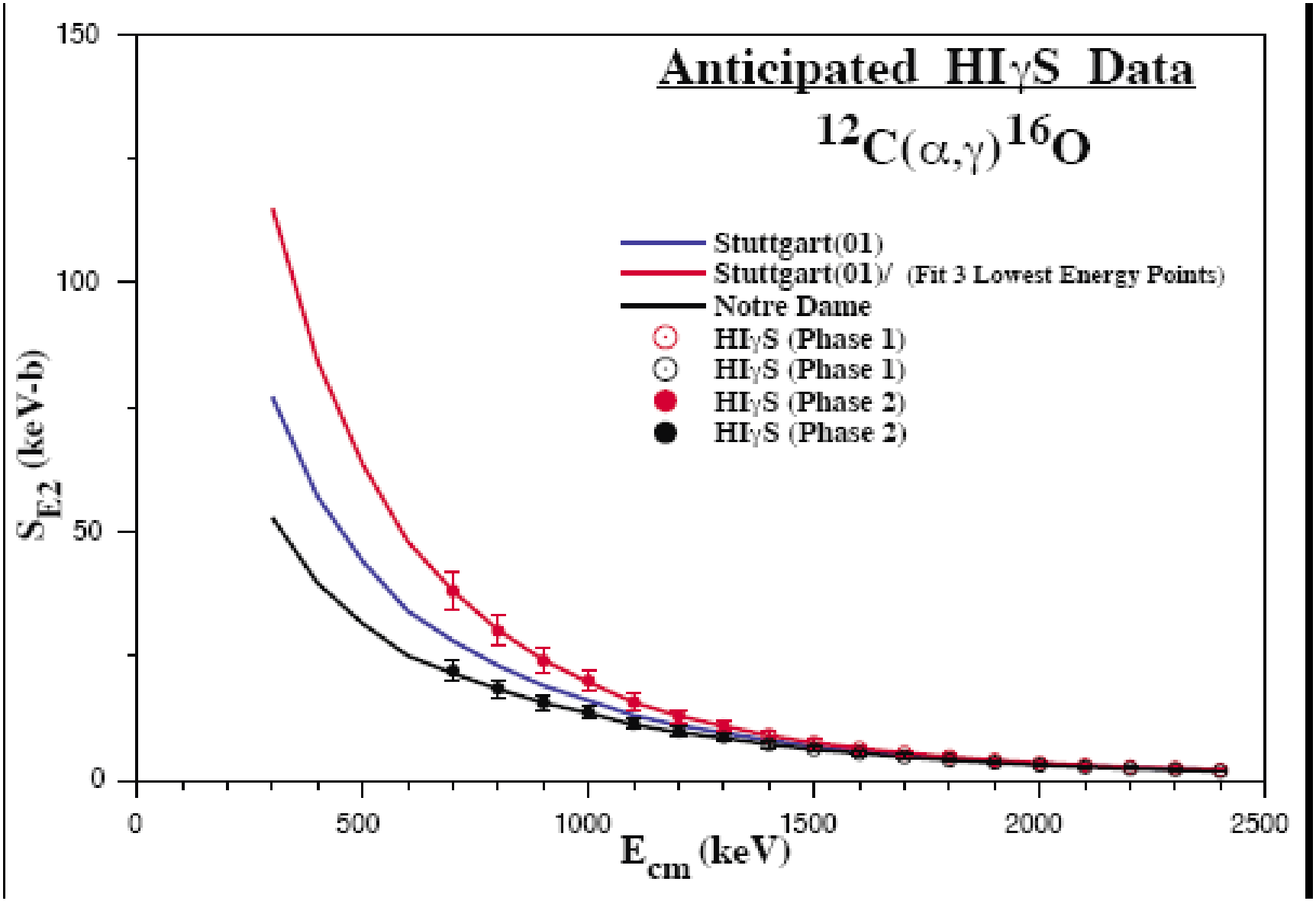
Anticipated HIγS Data
$^{12}C(\alpha,\gamma)^{16}O$
Stuttgart(01)
Stuttgart(01)/ (Fit 3 Lowest Energy Points)
Notre Dame
HIγS (Phase 1)
HIγS (Phase 1)
HIγS (Phase 2)
HIγS (Phase 2)
S_{E2} (keV-b)
E_{cm} (keV)
150
100
50
0
0
500
1000
1500
2000
2500

Phases obtained from recent (EUROGAM) angular distributions disagree with those from elastic scattering (PRC 73, 055801 (2006))

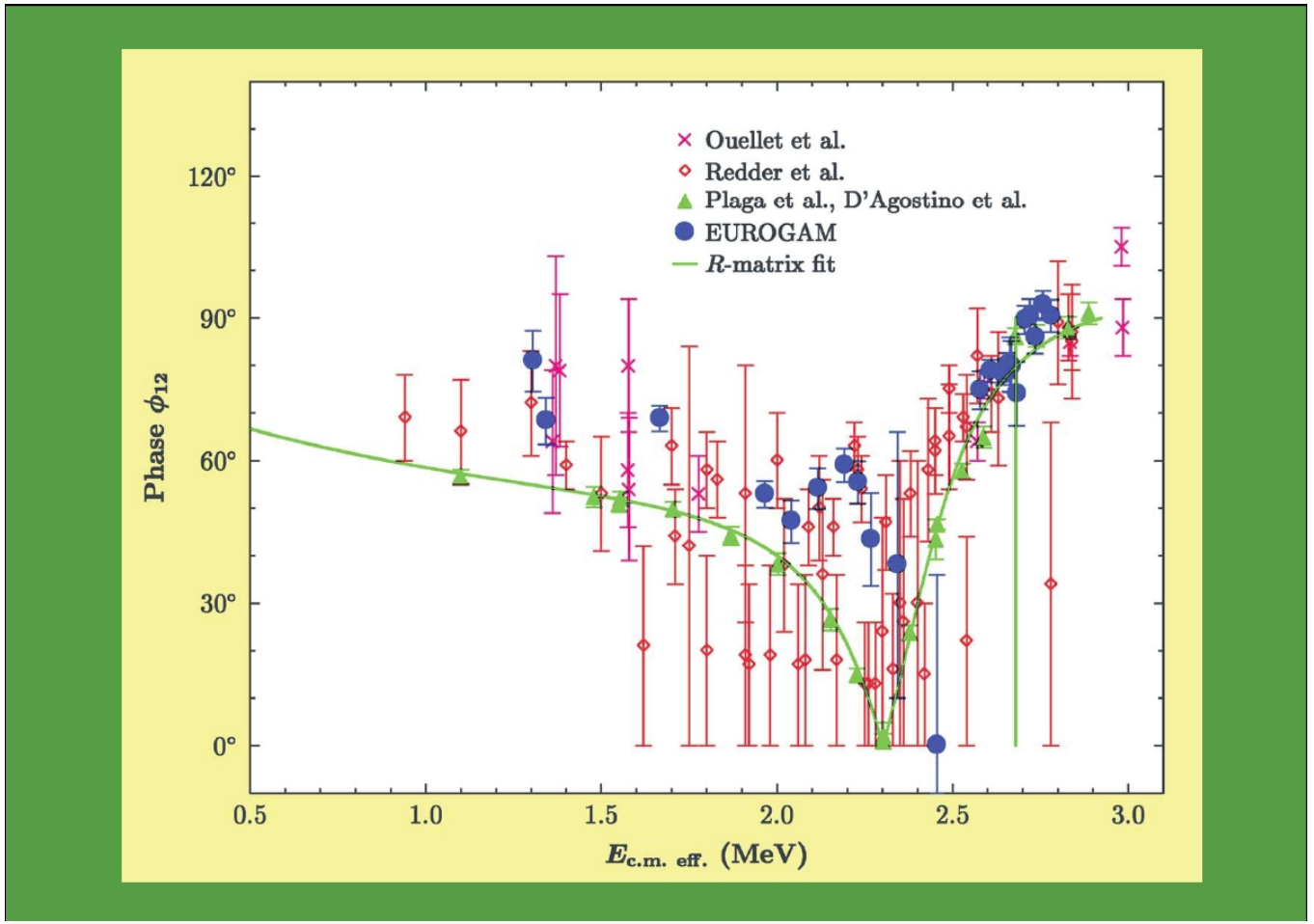

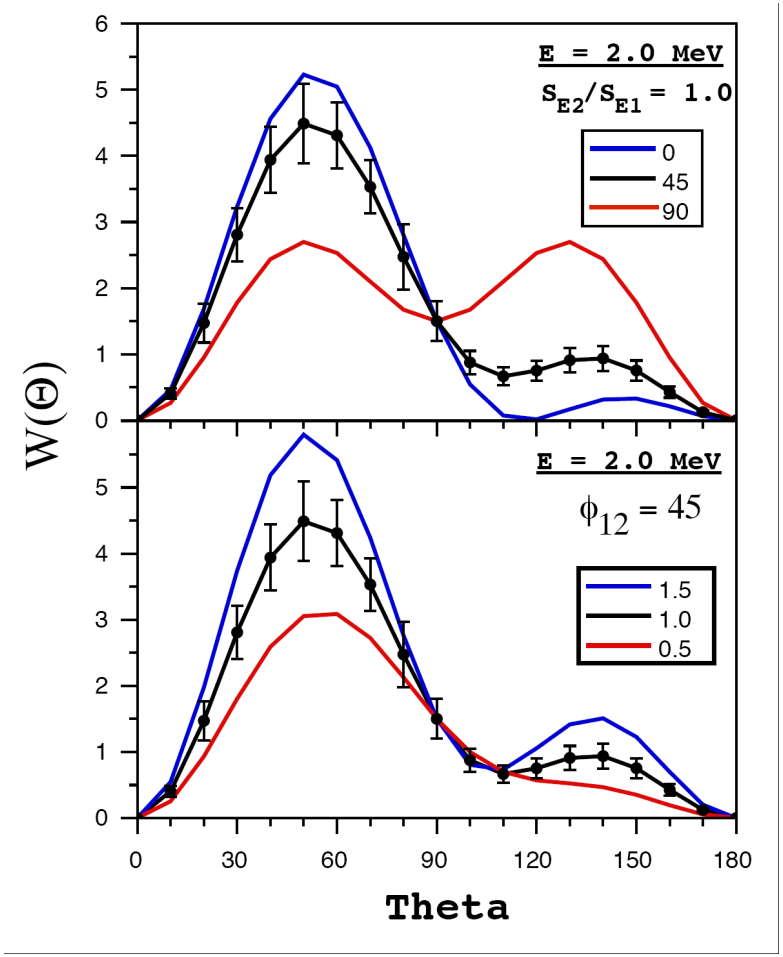
E = 2.0 MeV
S_{E2}/S_{E1} = 1.0
0
45
90
E = 2.0 MeV
ϕ_{12} = 45
1.5
1.0
0.5
W(Θ)
Theta
0
30
60
90
120
150
180
0
1
2
3
4
5
6

Projected HIγS data for 32 hours of running. *Eurogam* result is from Assuncao et al. PRC 73, 055801 (2006).

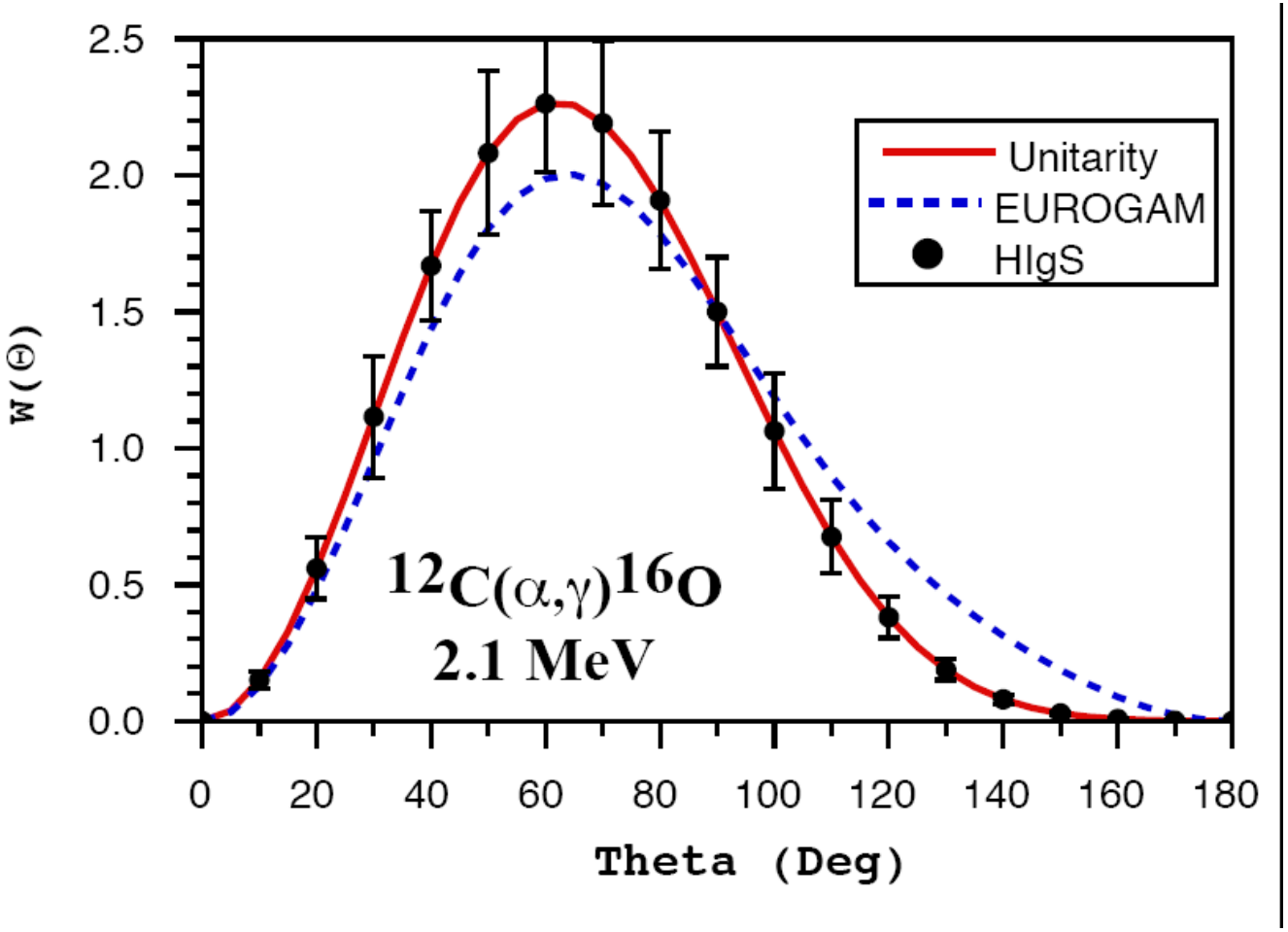

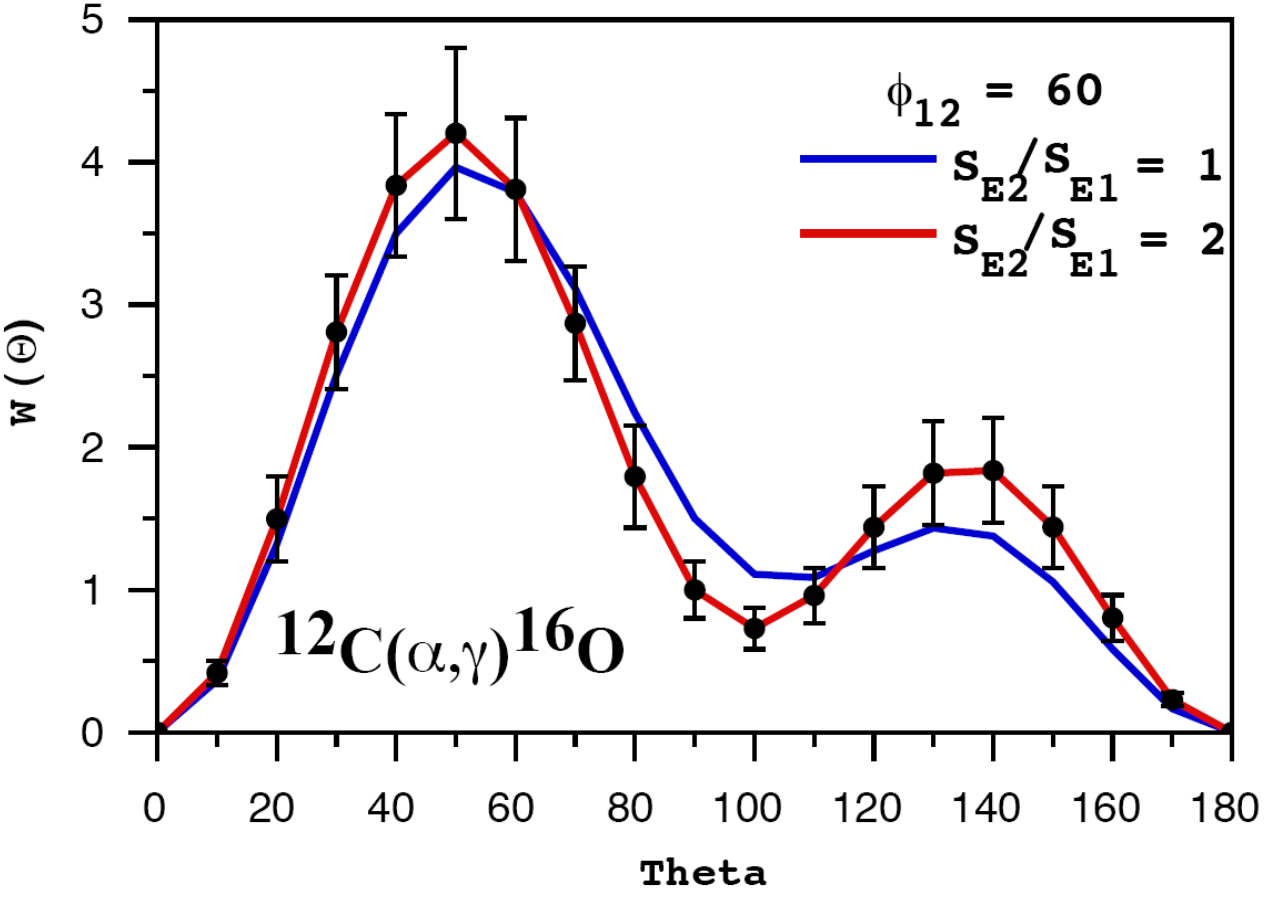
ϕ_{12} = 60
S_{E2}/S_{E1} = 1
S_{E2}/S_{E1} = 2
$^{12}C(\alpha,\gamma)^{16}O$
W (Θ)
Theta
0
1
2
3
4
5
0
20
40
60
80
100
120
140
160
180

Study of the triple alpha reaction

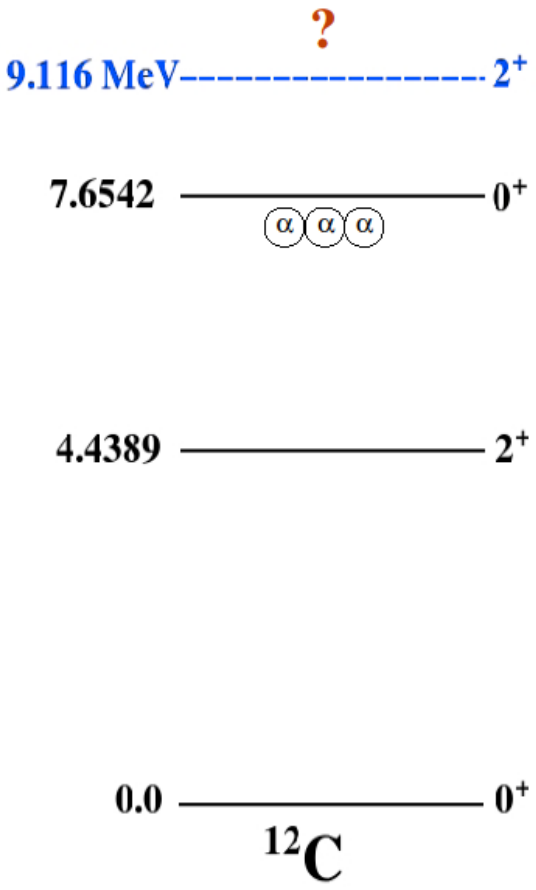

- 2^+ at 9.116 MeV was predicted by Descouvemont and Baye, Phys. Rev. C**36**(1987)54. (as a member of the rotational band built on top of the deformed 0^+ state at 7.6542)
- It was included as part of the NACRE compilation, C. Angulo et al., Nucl. Phys. **A656**(1999)3.
- Evidence for a broad 2^+ state ~10 MeV was found by M. Itoh et al. in $^{12}C(\alpha,\alpha')$, Nucl. Phys. **A738**(2004)268.
- No evidence for a broad 2^+ state ~10 MeV was found by the ISOLDE collaboration in the β-decay of ^{12}B and ^{12}N, Nature **433**(2005)136, Nucl. Phys. **A760**(2005)3.

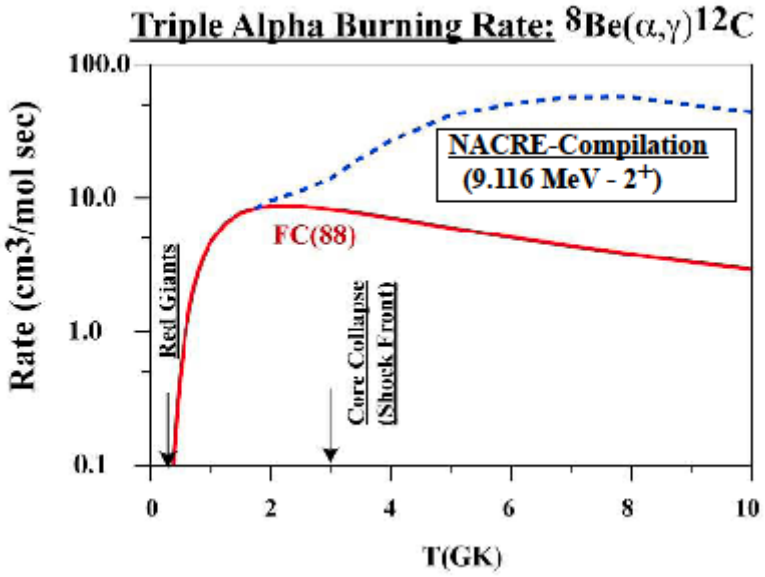
Triple Alpha Burning Rate: $^{8}Be(\alpha,\gamma)^{12}C$
Rate (cm3/mol sec)
100.0
10.0
1.0
0.1
0
2
4
6
8
10
T(GK)
NACRE-Compilation
(9.116 MeV - 2^{+})
FC(88)
Red Giants
Core Collapse
(Shock Front)

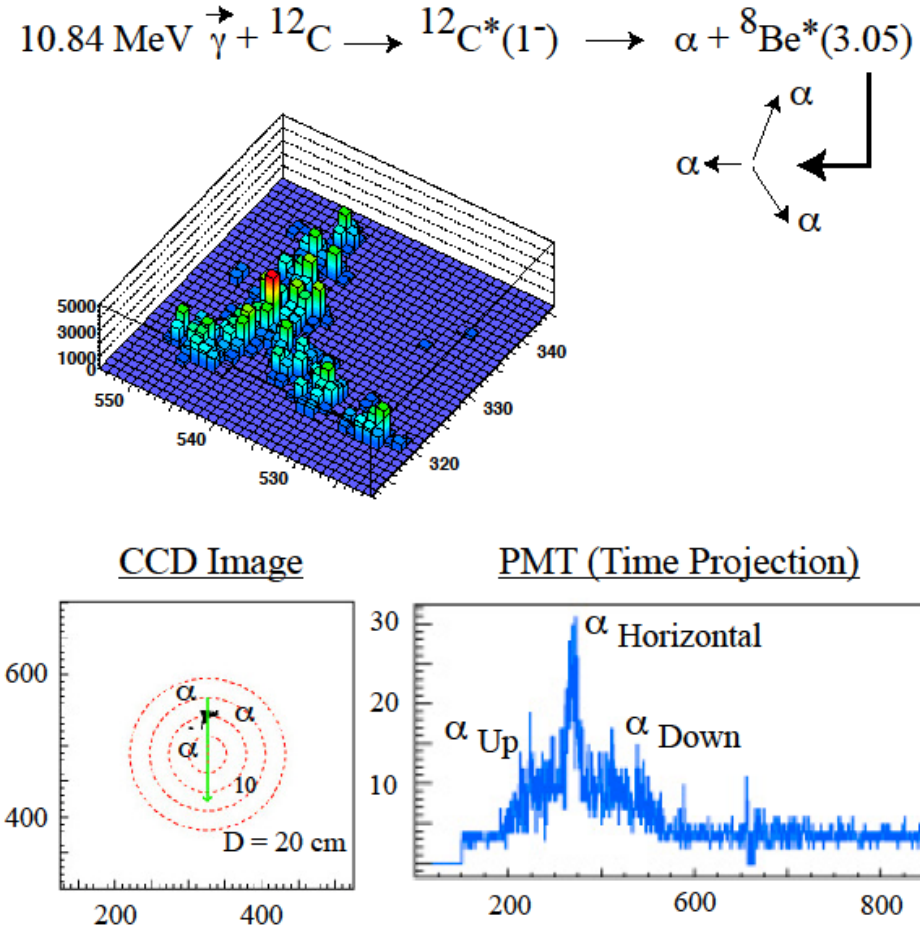
10.84 MeV γ + 12C → 12C*(1-) → α + 8Be*(3.05)
α
α
α
5000
3000
1000
0
550
540
530
340
330
320
CCD Image
PMT (Time Projection)
600
400
200
400
α
α
α
10
D = 20 cm
30
20
10
α Horizontal
α Up
α Down
200
600
800

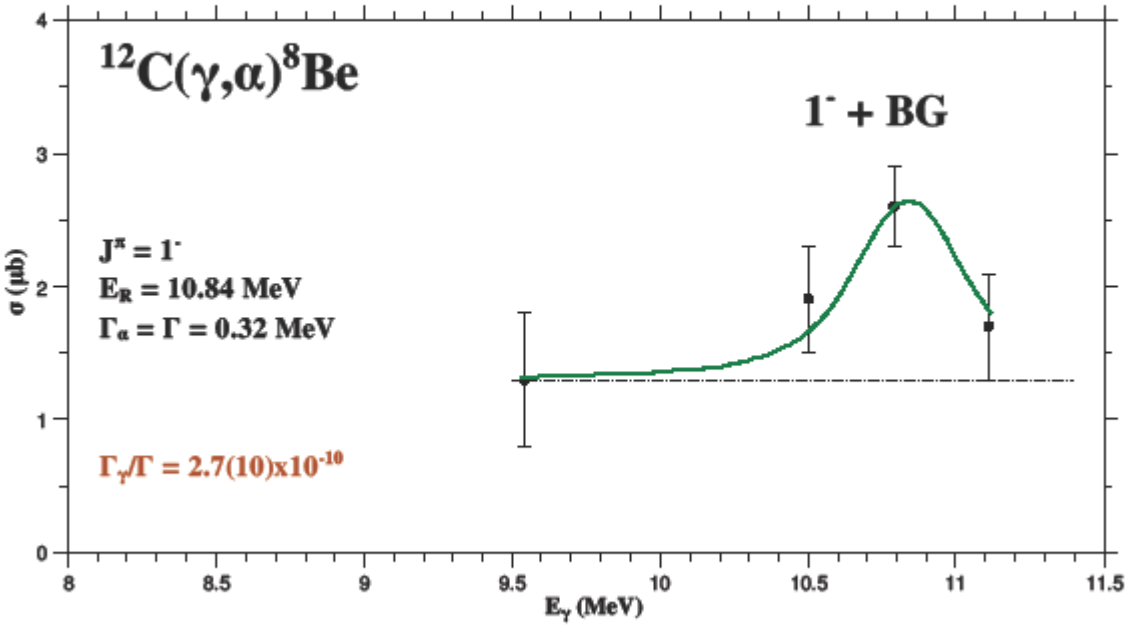
$^{12}C(\gamma,\alpha)^{8}Be$
$1^- + BG$
$J^\pi = 1^-$
$E_R = 10.84$ MeV
$\Gamma_\alpha = \Gamma = 0.32$ MeV
$\Gamma_\gamma/\Gamma = 2.7(10)\times10^{-10}$
σ (μb)
E_γ (MeV)
0
1
2
3
4
8
8.5
9
9.5
10
10.5
11
11.5

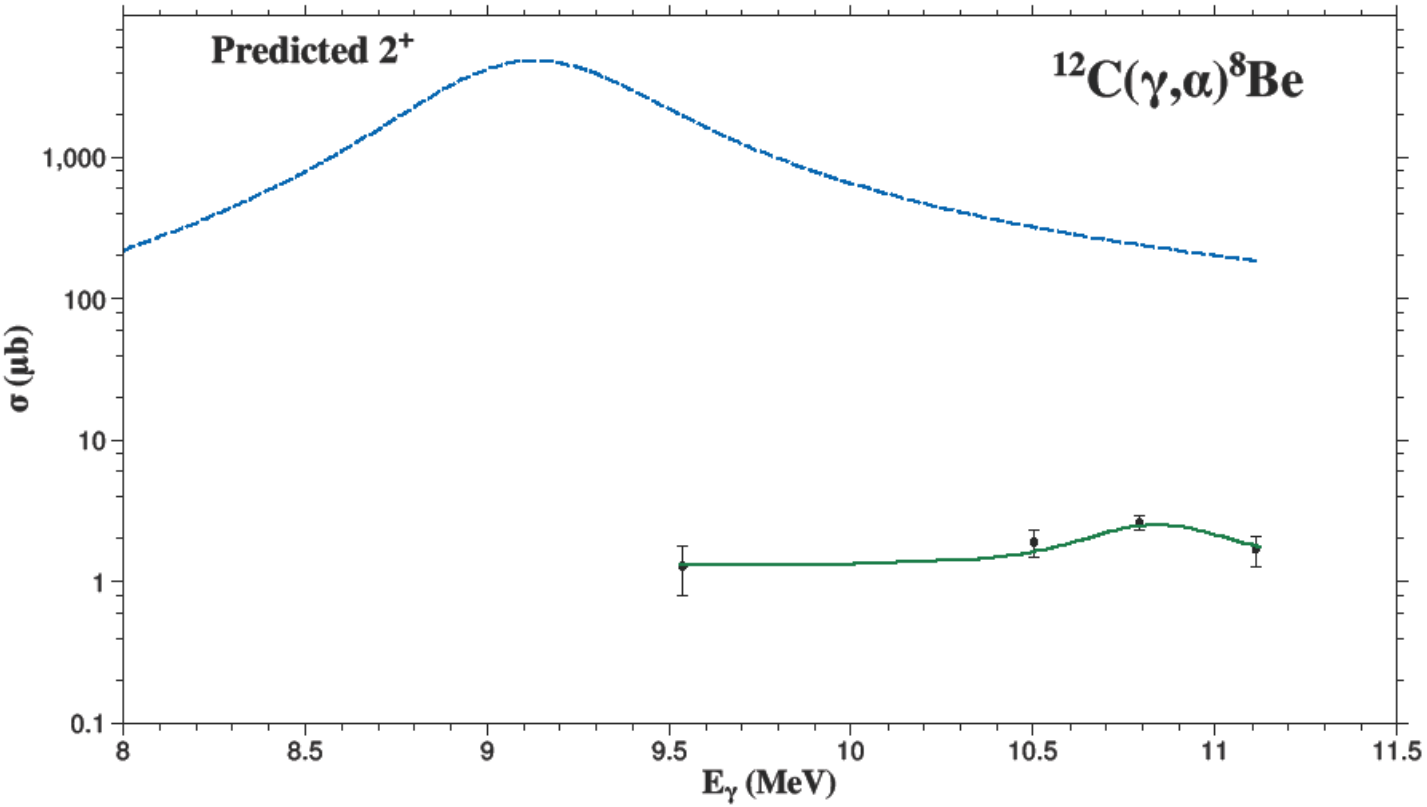
Predicted 2+
12C(γ,α)8Be
1,000
100
10
1
0.1
σ (μb)
8
8.5
9
9.5
10
10.5
11
11.5
Eγ (MeV)

Conclusions:

The cross section for $^{12}C(\gamma,\alpha)^{8}Be$ was measured to be at least two orders of magnitude lower than that predicted by Descouvemont and Baye for a broad 2^+ state at 9.116 MeV.

- **Does the predicted 2^+ state exist?**
- **If yes, it must have an anomalously low B(E2) ($< 10^{-3}$ W.u.).**
- **Along with the non-observation in β-decay, we may suggest that the predicted 2^+ state does not exist.**
- **Does the predicted rotational band built upon the deformed 0^+ state exist?**

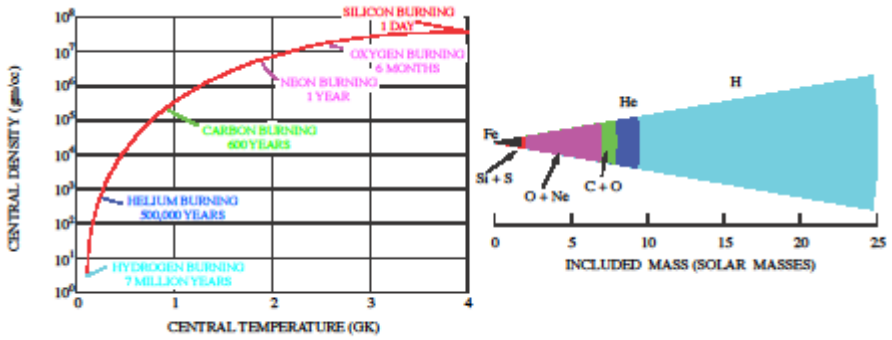

Bethe & Brown, 1985 (x10)

Mirror Testing Program (780 – 230 nm)

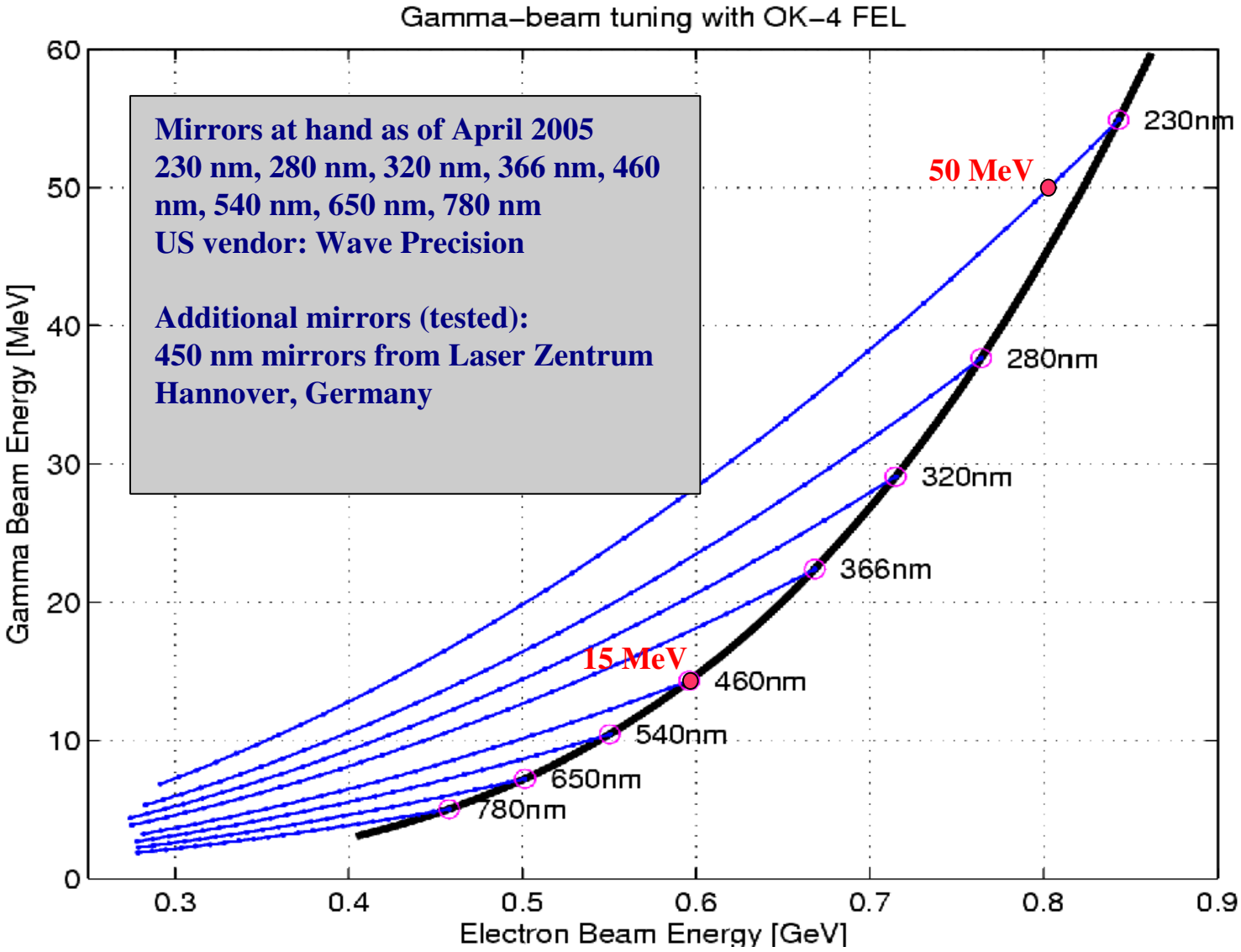

Two Bunch Mode

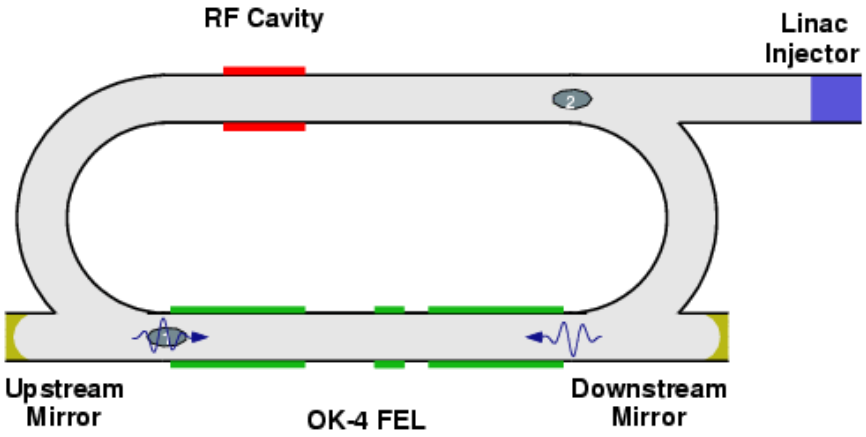

Created by Brent Perdue, 2005

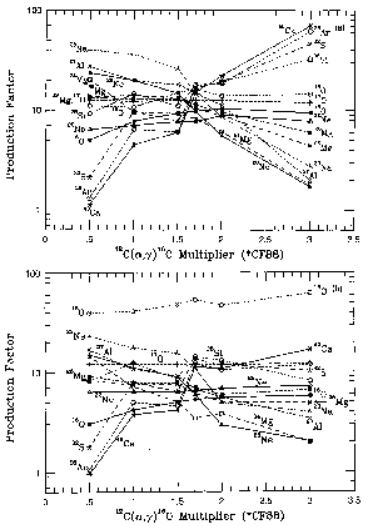

Fig. 4. Production factors for 14 isotopes of elements from oxygen through calcium as a function of $^{12}C(\alpha,\gamma)^{16}O$ reaction rate for models having a "nominal" amount of semiconvection (a) and "restricted" semiconvection (b). Each point represents an average over an initial stellar mass function of a grid of stellar masses (see text). Best agreement with solar abundances is achieved if the $^{12}C(\alpha,\gamma)^{16}O$ rate has a value near 1.7 times that given by CF88. Additionally, a substantial amount of semiconvection seems to be required in order that ^{18}O not be overproduced.

nearly identical ($1.6 - 0.7$ versus $1.7 + 0.5$). These results suggest that the nucleosynthetic effects of the $^{12}C(\alpha,\gamma)^{16}O$ reaction are mostly independent of semiconvective mixing rate, as is the "nucleosynthetic" prediction for its rate given above.

What is the significance of the order of magnitude overproduction of ^{18}O relative to the mean of the rest of the isotopes in the restricted convection case? On the surface, this overproduction seems to be an excellent discriminant in favor of the "nominal" semiconvection rate. It occurs over the entire range of stellar masses considered and shows only a small dependence on the $^{12}C(\alpha,\gamma)^{16}O$ rate, as can be seen from tables 7 and 8 and fig. 4b.